MODELING AND DESIGN OF AN ELECTRICAL MOWER DECK CONTROL SYSTEM

A Thesis

Submitted to the Faculty

of

Purdue University

by

Li Fu

In Partial Fulfillment of the

Requirements for the Degree

of

Master of Science in Electrical and Computer Engineering

May 2020

Purdue University

Indianapolis, Indiana

THE PURDUE UNIVERSITY GRADUATE SCHOOL
STATEMENT OF THESIS APPROVAL

Dr. Lingxi Li, Chair

Department of Electrical and Computer Engineering

Dr. Yaobin Chen

Department of Electrical and Computer Engineering

Dr. Stanley Chien

Department of Electrical and Computer Engineering

Approved by:

Dr. Brian King

Head of School Graduate Program

ACKNOWLEDGMENTS

Many thanks go to my whole family who supported me to accomplish my thesis. Being a mother of three children, I get so many happy feelings and much energy from them. Without my husband's help and support, I would not be able to finish this thesis. Without the support of my children, I would not have had enough time to meet this goal. I am also very thankful to my parents and my husband's parents. You all always contribute a lot to my family, which has enabled me to put all my energy into finishing my master's degree.

I am also very thankful to my supervisor, Scott Windhorst, and to my colleague, Jesse Welling, who are both at Hydro-Gear. They gave me a lot of support and suggestions. Without encouragement and guidance from my advisor, Dr. Lingxi Li, I do not think I can finish my thesis.

I also would give my thanks to TASI, as well as Dr. Yaobin Chen and Dr. Stanley Chien. Dan Shen and Wensen Niu. They gave me a lot of help when I started writing this thesis.

With the help of Sherrie Tucker, our department's assistant and my friend, Lars Magnusson, the grammar of my thesis has been greatly improved.Thanks to everyone who helped and supported me.

TABLE OF CONTENTS

Page

LIST OF TABLES

LIST OF FIGURES

Figure Page

Figure Page

ABBREVIATIONS

BLDC	Brushless DC Motor
PMSM	Permanent Magnetic Synchronous Motor
SVM	Space Vector Modulation
PWM	Pulse Width Modulation
SPWM	Sinusoidal Pulse Width Modulation
SVPWM	Space Vector Pulse Width Modulation
FOC	Field Oriented Control
PID	Proportional Integral Differential
UART	Universal Asynchronous Receiver/Transmitter

ABSTRACT

Fu, Li. M.S.E.C.E., Purdue University, May 2020. Modeling and Design of An Electrical Mower Deck Control System. Major Professor: Lingxi Li Professor.

With the development of the electric mower, an electrical control system is necessary to drive the blades and the traction wheel. This thesis introduces an electrical deck control system. The system includes a high-powered deck controller and a permanent magnet synchronous motor (PMSM). A PMSM control model has been built in MATLAB/Simulink to verify and support the physical design. Three different PWM modulation methods have also been implemented and compared in MATLAB/Simulink. Furthermore, a model for the distribution and features of grass was built based on sampling of Google Street View images. A six-step pulse width modulation (PWM) control strategy was realized using a PIC33 embedded microprocessor. An enhanced closed-loop control system design was implemented to keep a constant blade speed in order to cut grass efficiently.

1. INTRODUCTION

A lawn mower is defined as a machine or an equipment that utilizes a revolving blade to cut the turf-grass to a certain height [1]. Lawn mowers are penetrated into our lives. People want to keep a beautiful habitat environment [2]. The exponential increases in commercial construction activities and demand for backyard beautification among households are pushing the growing market of the lawn mower in US, especially for the electric mower [3]. The United States Lawn Mower Market Analysis Forecasts 2019-2024 shows that the revenues of the lawn mower market in the U.S. will reach approximately $13 billion by 2024, and the growth rate is predicted to be around 4% during 2018-2024 [4].

Figure 1.1 shows some common types of mowers classified based on operation mode. These include the push mower, the standing mower, the riding mower, tractor-pulled mower and autonomous robotic mower based on the operation mode. Mowers can also be classified based on by blade rotation: cylinder/reel and rotary mower are shown in Figure 1.2. The cylinder/reel mower carries a horizontal cutting blade at the desired cutting height. The rotary mower rotates one or more vertical axis with the blades spinning at a very high speed to generate enough impact to cut the grass [1]. From the view of the power source, lawn mowers can be classified by gasoline-powered or electricity-powered mower. Most rotary push and riding mowers are currently powered by internal combustion engines (gasoline-powered), with the engine power for rotary push mowers normally ranging from 4 to 7 horsepower [1].

With electric technical development, more and more electric mowers appear in the market. Electric mowers can be divided into Battery powered, Solar energy powered and utility powered (corded). The electric mower has more advantages than the traditional gas engine mower for developing sustainable cities and protecting the eco-system, the electric mower has more advantages than the traditional gas engine

mower. Furthermore, The autonomous (robotic) lawn mower has the most potential to be the winner in the future mowing application market.

Figure 1.1. Mower classification based on operation mode

Reel mower

Rotatry mower

Figure 1.2. Mower classification based on blade rotation

1.1 The Battery Powered Electric Mower

The lawn mower is transitioning from combustion engine mower era into the new electric mower era because of several advantages of electric power. Air pollution is the major concern related to the conventional gas powered lawn mower. A study showed that some gas powered lawn mowers can generate the same amount of air pollution in one hour as driving a vehicle for 650 miles [5]. Moreover, the mower produces significant noise pollution [6] [7] which can cause hearing loss if the operator is not wearing hearing protection. As a result, about one million people working in ground-keeping and lawn service suffer occupational hearing problems. A recent study found that the noise level produced by push mowers is between 86-95 decibels, while it can reach 96 dB for a riding mower. Both of these exceed the limit of 85 dB (8-hour time-weighted average) recommended by the National Institute for Occupational Safety and Health (NIOSH) [8].

To reduce the possibility of air pollution and noise pollution, electric mowers were developed and have been widely used in recent years. In this thesis, a deck control system for the battery-powered electric mowers was developed. It should be noted that the control system for an electric mower includes a control panel, a battery management system, a wheel controller and a blade controller. The deck control system in this thesis specifically deals with the blade controller.

1.2 The Riding Rotary Mower

As mentioned above, mowers are classified in to four different types, which are the push mower, the standing mower, the riding mower and the autonomous (robotic) mower based on operation modes and power levels. In this thesis, the research is focusing on the high power riding mowers. Furthermore, the focus is on the rotary mower, as opposed to the cylinder (or reel) mower. Figure 1.3 shows the basic structure of the riding rotary mower.

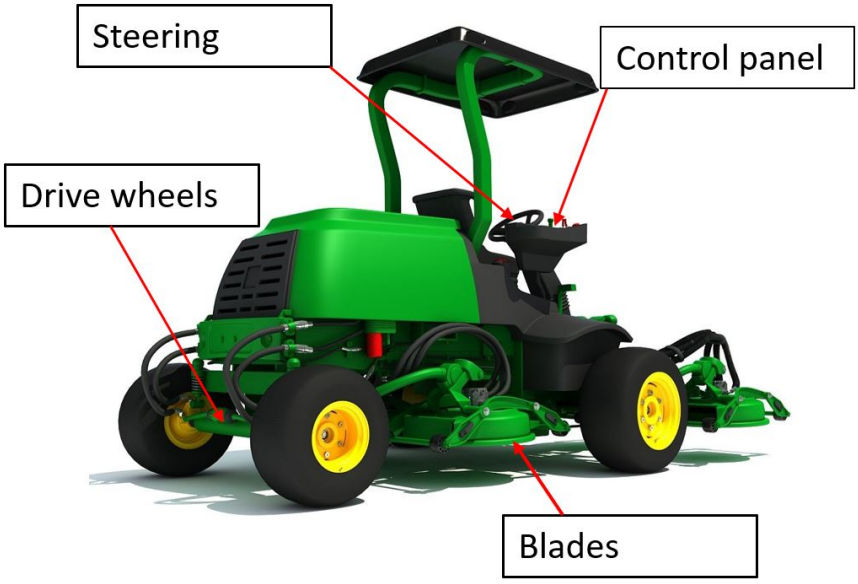

Figure 1.3. The structure of the riding rotary mower

As seen in Figure 1.3, the riding rotary mower consists of four key parts in terms of the control system. They are the control panel, two rotary blades, the steering system and four drive wheels. The goal of this research design is to design a deck control system, focusing on the blade speed control when the blade is powered by a permanent magnet synchronous motor.

1.3 The Permanent Magnet Synchronous Motor

An electric motor converts electrical energy to mechanical energy. There are many different types of motors. Typically we classify the motor based on AC or DC driving. Because of limitations of power electronics, such as switching frequency, it was very hard to obtain the accurate speed for AC motors. With improvements in electronic technology, Brushless DC (BLDC) and Permanent Magnet Synchronous Motors (PMSM) are widely used in many applications such as landscaping, industry, aerospace and appliances. Meanwhile BLDC/PMSM have many advantages such as no brush, wide range of speed control, and impact volume with high power density.

Motor classification in terms of motor type is shown in Figure 1.4. [9] involves a research of the comparison between BLDC motor, PMSM motor and other types of motors and supports that permanent magnetic motors has characteristics of the high power density, higher speed and higher efficiency.

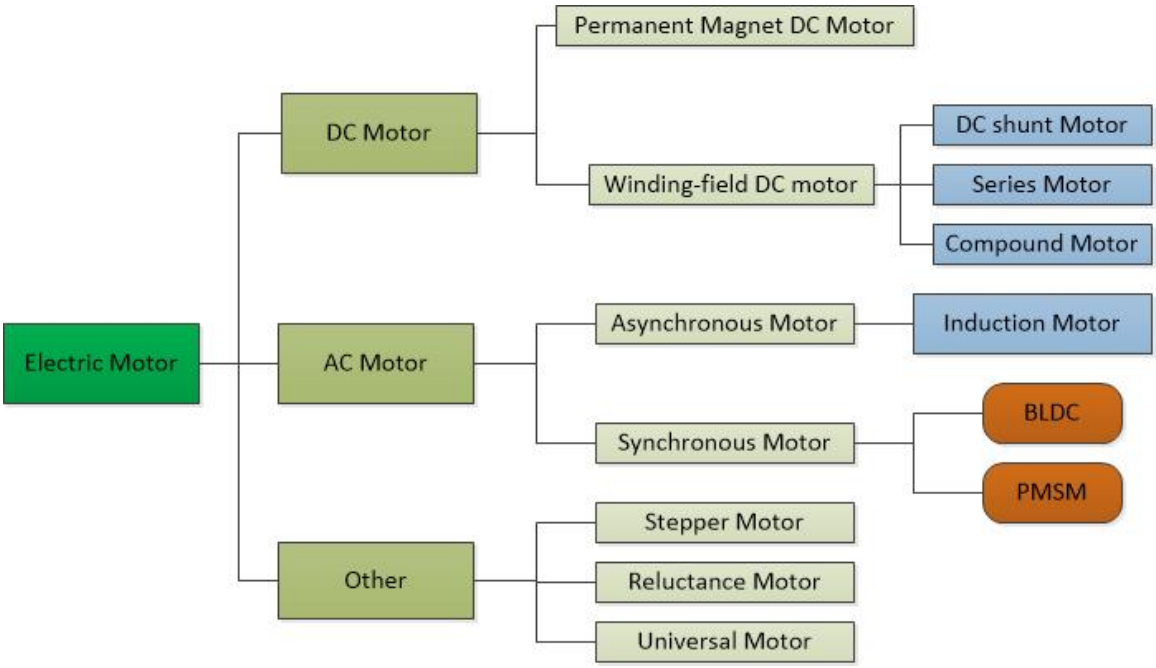

Figure 1.4. Motor classification based on AC/DC current supply

Considering these advantages and sustainable development, a PMSM was chosen as the drive motor for the deck control system.

1.3.1 BLDC

The BLDC motor used in a deck control system is a BLDC 3-phase synchronous motor which includes a static winding stator and a permanent magnetic rotor. The brushless DC motor is not actually a DC motor, but is driven by direct current (DC) electricity. BLDC has trapezoidal back EMF, so typically BLDC is driven by electronically commutating in three windings instead of mechanically commutating using brushes.

1.3.2 PMSM

PMSM is physically similar to BLDC. Both commonly have a magnetic rotor and three-phase windings. PMSM distributes sinusoidal flux density in the air gap instead of trapezoidal flux density.

For the permanent magnetic motor, rotors are classified as salient pole rotors and non-salient pole rotors based on magnets installation. In Figure 1.5, (a) is a non-salient rotor because arc magnets are glued to the surface of the rotor. Rotors (b) and (c) are salient machines which means that Ld and Lq are different. Rotor (b) is cylindrical in shape, having parallel slots on it to place magnets. Rotor (c) is the typical Interior Permanent Magnet (IPM) machine, in which the magnet is inserted in the rotor body. When the Lq/Ld ratio is close to 1, type (b) can be treated as a non-salient motor. Because the ratio of the IPM motor can reach up to 3 [10], the flux weakening method can be used in IPM motor control [11] to achieve higher speed control.

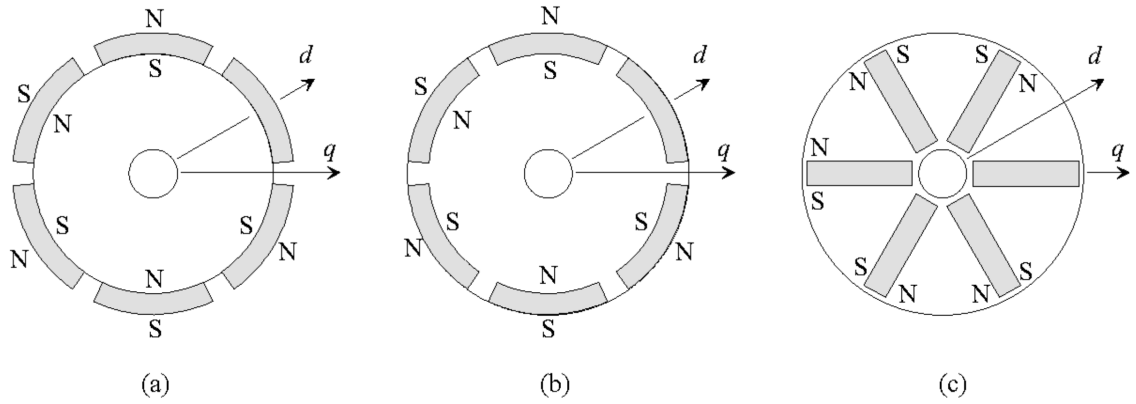

Figure 1.5. Motor classification based on magnet location

1.4 Grass Classification

Mowing is the most important aspect of maintaining the quality and beauty of the lawn. A proper mowing practice, along with routine irrigating and fertilizing,

can increase the density of turf grass and prevent the growth of weeds. Two factors that affect mowing practices are cutting height and frequency. Unlike on traditional gas-engine driven mowers, blade speed and cutting torque can be easily controlled on electric mowers. To have an optimum cutting height, the blade speed should be variable, depending on the growth status of the turf grass. The first important factor which could affect the control strategy of the blade is the turf grass species and cultivar. Normally, a grass that spreads horizontally can be mowed shorter than an upright-growing, bunch-type grass. For example, Bahiagrass should be mowed to a taller height because of its upright growth habit. On the other hand, Bermudagrass needs to be mowed at a very low height because of its narrow leaf. Another factor which could affect the blade torque significantly is the portion of yellow turf grass compared to green turf grass. Usually, the yellow turf grass is withered, and is much dryer than the green grass. From the view of blade control, less torque is needed. To enable development of an optimized control strategy, turf grass was be studied and modeled. The study was originally conducted by TASI (Transportation Active Safety Institute) at IUPUI (Indiana University-Purdue University, Indianapolis) [12]. More details will be discussed in Chapter 2.

1.5 The Objective of this Research

As mentioned in Section 1.2, a deck control system has been designed in this thesis. It should be noted that for the purposes of this thesis, the deck control system specifically deals with blade speed control. The blade is powered by a permanent magnet synchronous motor. To achieve an optimal control strategy, the motor, the three-phase bridge/commutation logic, and turf grass were modeled and simulated in Chapter 2. The hardware system design and software system design were conducted in Chapter 3 and Chapter 4, respectively. Bench experiments and results are described in Chapter 5 and conclusions are drawn and presented in Chapter 6.

1.6 Contributions

The contributions of this thesis are stated as follows:

- A PMSM model was built to understanding how to use PMSM in the control system.
- A MATLAB/SIMULINK model of a closed-loop speed control system using a six step PWM control algorithm was developed.The model is very beneficial for future physical design.
- Extended another model of a PWM control algorithm, Space Vector Pulse Width Modulation, which has several advantages such as less harmonic distortion, greater efficiency and less switching loss.
- The grass model was analyzed which is beneficial for defining the load torque of the control system.
- Hardware, software and communication were implemented for a deck control system of an electric mower. Multiple key components were optimized to adapt to size and cost requirements.

2. CONTROL SYSTEM MODELING

In order to design a proper motor control system, it is very useful and helpful to build a mathematical model of the whole control system, which includes the PMSM model, three-phase full-bridge model and commutation sequence and turf grass model.

2.1 System Requirements

Currently, the control system power is battery-powered. Power supplies with voltage 24V, 48V, 60V and 75V are available. In this project, a 48V power supply was dedicated as the power source of the whole system. The length of the cutting blades is 50cm and the inertia is about 0.03 $kg.m^2$. In terms of requirements, the basic specifications are as follows:

Table 2.1. System and Motor Specification

Rated Voltage	48V
Continuous Current	30A
Continuous Speed	3000 RPM
Continuous Load torque	4 Nm
Terminal Resistance	10 mΩ
Terminal Inductance	80 μH
Continuous output power	1.5 KW
Torque constant	0.13 Nm/A
Pole pairs	5

2.2 PMSM Modeling

A permanent magnet synchronous motor (PMSM) uses permanent magnets to produce the air gap magnetic field instead of using electromagnets [13]. The B-H curve illustrates the magnetic properties of magnetic materials. It tells how the magnetic material responds to an external magnetic field force, which is an important aspect of permanent magnet motor design. Use of rare earth permanent magnetic materials can make the motor smaller and lighter because of its strong magnet performance. However, rare earth magnets are comparatively expensive. Hardened steel was used at the earliest time. It is easy to magnetize but cannot hold low energy [13]. Figure 2.1 illustrates different magnet materials. Neodynium-iron-boron(NdfeB) is the most commonly used rare earth magnet material because of its strong permeability and its ability to remain magnetic for a long time once it gets magnetized. As illustrated seen in Figure 2.1 (a), flux density will reach saturation when increasing magnetizing force in both directions. Figure 2.1 (b) shows the second quadrant curve of different materials. Ferrite has the biggest retentivity but has the smallest coercivity.

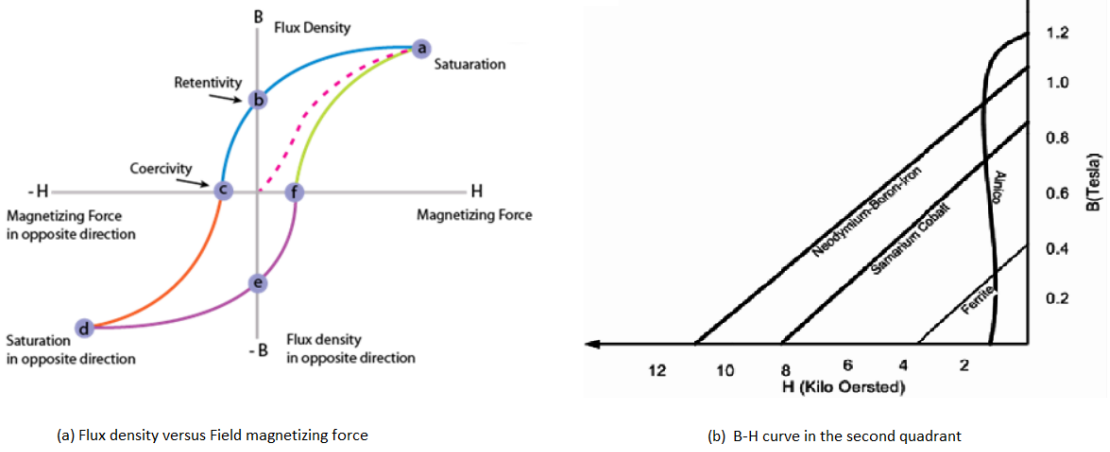

(a) Flux density versus Field magnetizing force

(b) B-H curve in the second quadrant

Figure 2.1. B-H curve [14]

It is necessary to introduce two important parameters k_e and K_t which are helpful to build the system transfer function. k_e represents the back EMF constant [15].

$$E = k_e \omega \tag{2.1}$$

Where, E — Phase Back emf.

ω — Electrical rotary speed.

In this control system, the back EMF of the motor shows in Figure 2.2. From Table 2.1, we can find the motor has five pole pairs. Using equation below, we can get the rotating speed. Moreover, k_e can be calculated.

$$\omega_n = 60f/p \tag{2.2}$$

Where,

f — rotational frequency.

p — Number of pole pairs.

ω_n — Mechanical rotation speed(rpm).

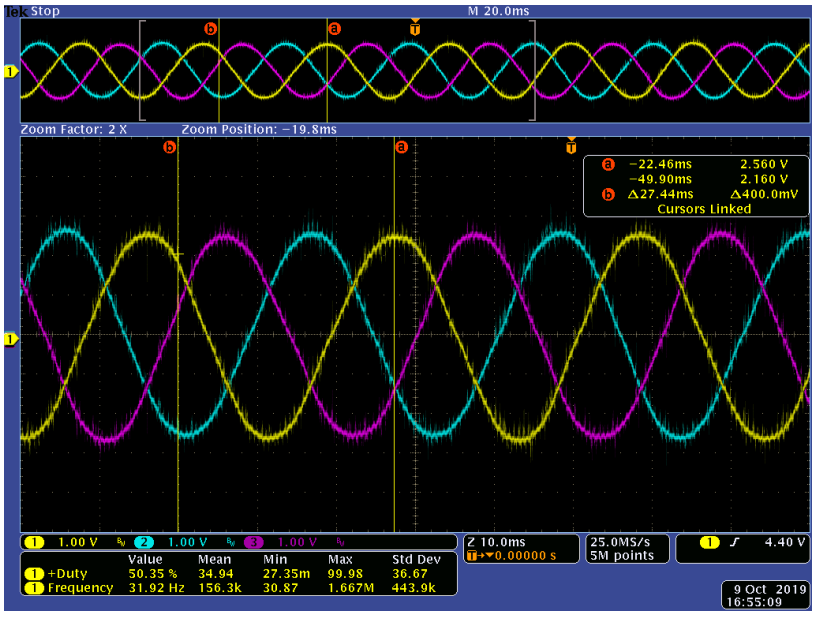

Figure 2.2. Three-phase back EMF of permanent magnetic synchronous motor

In the formula for torque(T),

$$T = k_T I \tag{2.3}$$

shows k_T is the torque constant and I is the current. Ideally, k_T =k_e, but one needs to pay attention to the unit. These two parameters were used when using the Laplace transfer function to induce the mathematical model.

PMSM can be regarded as 3 phase DC model tied at a common point. Figure 2.3 shows stator windings connecting as start pattern. The other pattern is delta pattern which is connected as a triangle. The three-phases are mathematically symmetrical.

$$\begin{cases} u_a = R_a i_a + (L_s - M)\dfrac{di_a}{dt} + e_a \\ u_b = R_b i_b + (L_s - M)\dfrac{di_b}{dt} + e_b \\ u_c = R_a i_c + (L_s - M)\dfrac{di_c}{dt} + e_c \end{cases} \tag{2.4}$$

Where,

L_s — the self inductance.

u — phase stator voltage.

M — mutual inductance.

i — phase stator current.

e — induced back-emf.

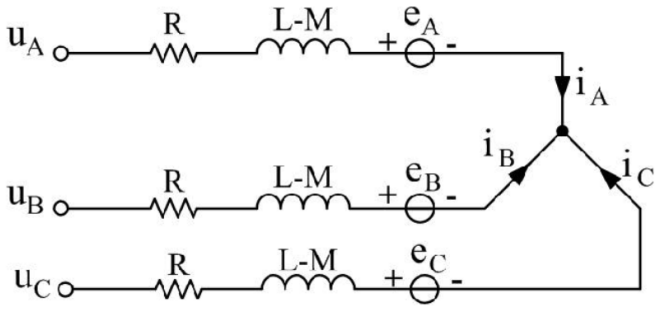

Figure 2.3. Equivalent circuits of the three-phase PMSM motor (assume Ld=Lq)

In the motor mechanical function equation, we get

$$T - T_d = J\frac{d\omega}{dt} + B\omega \tag{2.5}$$

Where,

T - Output torque

T_d - Load torque

J - Blade inertia

ω - Output speed (rad/s)

B - Friction constant

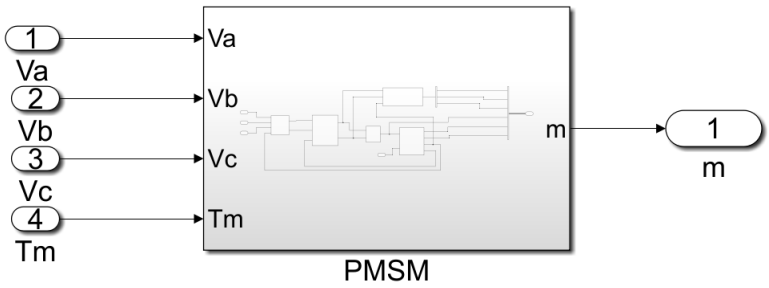

Figure 2.4. PMSM system block

Using the voltage equation, flux equation, torque equation and motion equation, the PMSM model was built (illustrated in Figure 2.4. Figure 2.5 shows the inner different function blocks such as dq transform, θ calculation and torque calculation. Three sinusoidal stator voltages have been decoupled to d and q axes in the PMSM model because transforming 3-axis to 2-axis is an efficient way to calculate the flux relationship between rotor and stator.

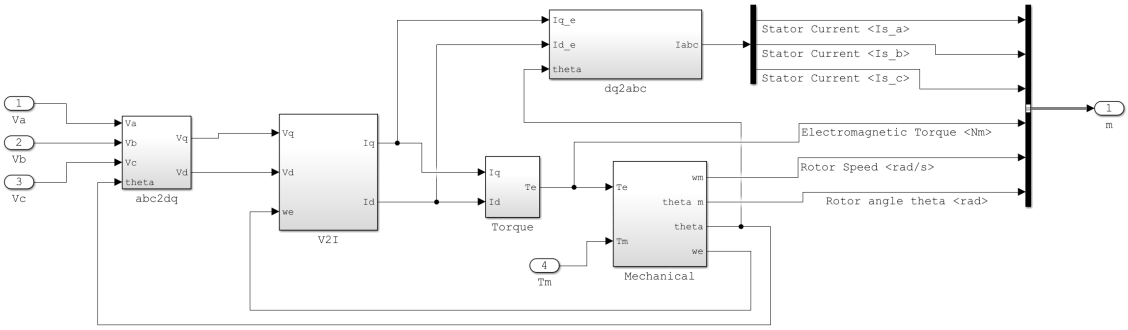

Figure 2.5. PMSM system block

There are five subsystems including Vd and Vq calculation, id and iq calculation, mechanical calculation, phase current calculation and Torque calculation. Using these five parts, we can build and simulate the PMSM.

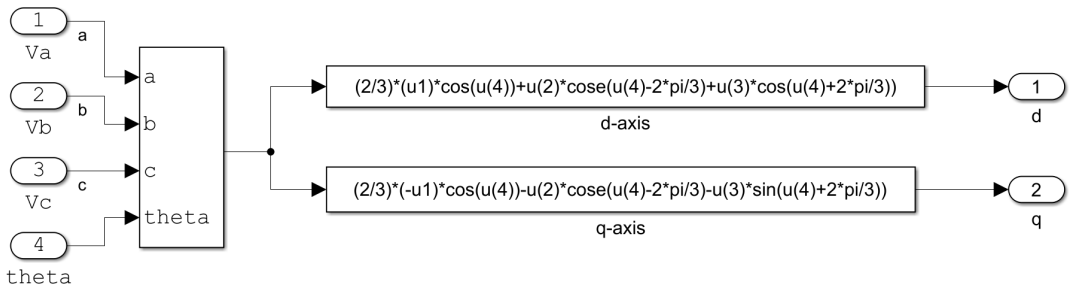

Figure 2.6. Vd and Vq calculation

Firstly, the Clarke transform function is used to transfer three-phase voltage to Vd and Vq, which coordinate with rotor position (Figure 2.6). After transforming, we use equation

$$\begin{aligned} \frac{di_d}{dt} &= \frac{u_d}{L_d} + \frac{L_q}{L_d}\omega i_q - \frac{1}{L_d}Ri_d \\ \frac{di_q}{dt} &= \frac{u_q}{L_q} - \frac{L_d}{L_q}\omega i_d - \frac{1}{L_q}Ri_d - \frac{\lambda}{Lq}\omega \end{aligned} \tag{2.6}$$

to get id and iq. Torque is proportional to current (showed in Figure 2.7). Based on the Motor mechanical function Equation 2.5, we get rotation angle and rotation speed.

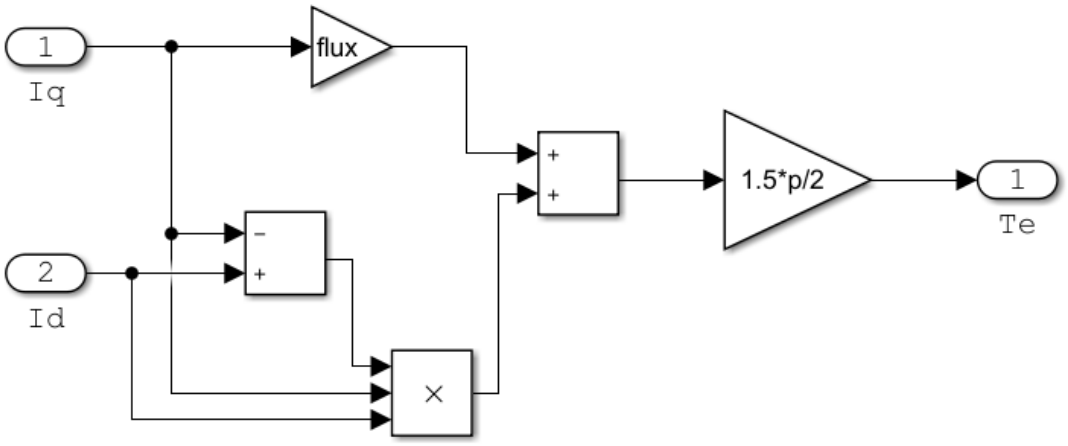

Figure 2.7. Torque calculation

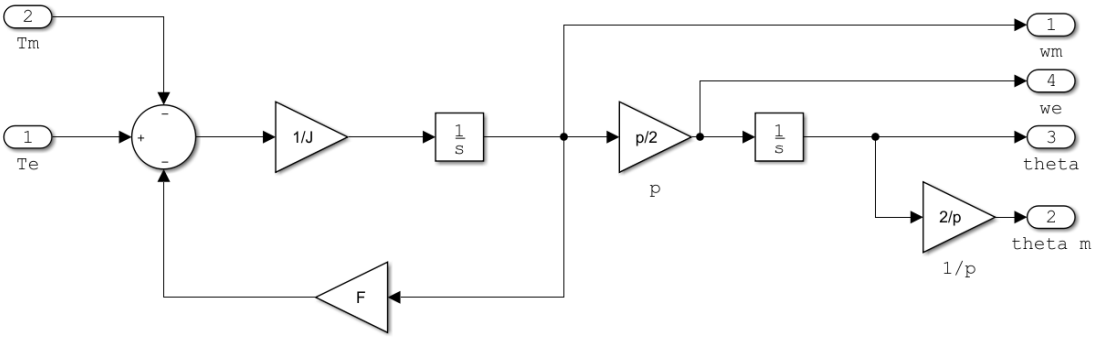

Figure 2.8. ω and θ calculation

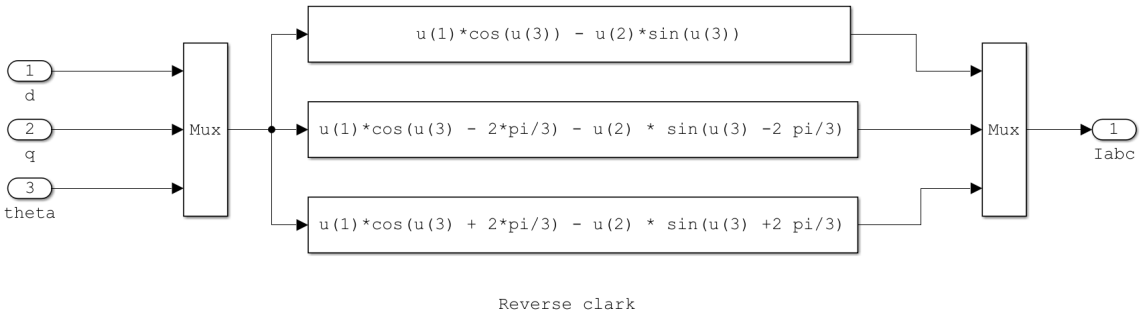

Figure 2.9. dq-axis to abc calculation

2.3 Braking Methodology

According to the standard of the mower (ANSI/OPEI B71.1-2017), generally The blades shall stop rotating from the manufacturer's specified speed within 5 seconds [ANSI/OPEI B71.1-2017, sec23.2]. There are several ways to stop the motor based on this requirement. The first is using inherent friction to stop the motor spinning. The disadvantage of this method is the significant amount of time it will take to stop if the rotor is large and the loads has a high moment of inertia.

To reduce downtime, or possibly as an emergency safety feature, DC injection braking can be used to quickly stop the rotor. The time duration for DC injection must be limited to prevent overheating of the rotor [16]. The brushless DC/AC motor also can be braked using short-circuiting its three-phase terminals. At this time, all kinetic energy will be dissipated in stator windings and (metal–oxide–semiconductor field-effect transistors) MOSFETs. The short allows high current to flow creating a magnetic field that opposes the rotor's field and produces the braking effect. Phase current curves indicates 100 Amps will be generated in 0.3s. Hence it definitely can meet the five-second stopping requirement. As long as the MOSFETs and motor wind can tolerate around a hundred amperes over a short period without sustaining damage, shorting phase will be the simplest and fast way to deal with the emergency braking situation.

2.4 Control Methodology and Commutation Logic

In the speed control system of the permanent magnet synchronous motor, different speed can be obtained, or speed kept constant when the load torque changes, by changing the voltage of the three-phase terminal. When the system was driven by a square wave, the harmonic amplitude of the voltage could not change. Pulse width modulation (PWM) will be introduced. Setting the fixable switching frequency and changing the duty cycle, we get the corresponding voltage of each terminal.

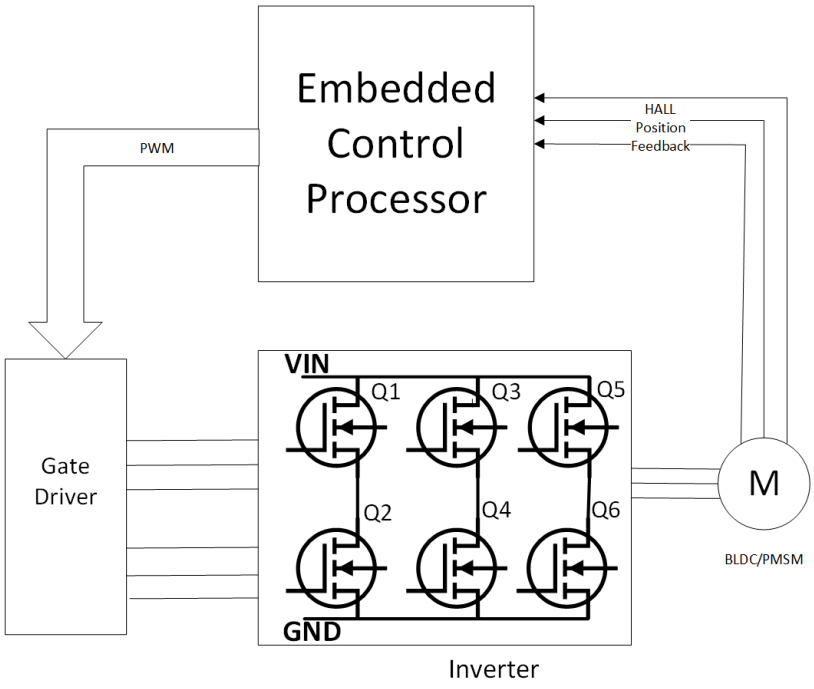

Figure 2.10. Sensored synchronous motor control diagram

2.4.1 Six-step PWM Control

Rotor rotation is influenced by the revolving stator poles, so the rotor pole position must be tracked in order to effectively drive three stator phases. Hence, a motor controller is used to generate a 6-step commutation pattern on three stator phases.

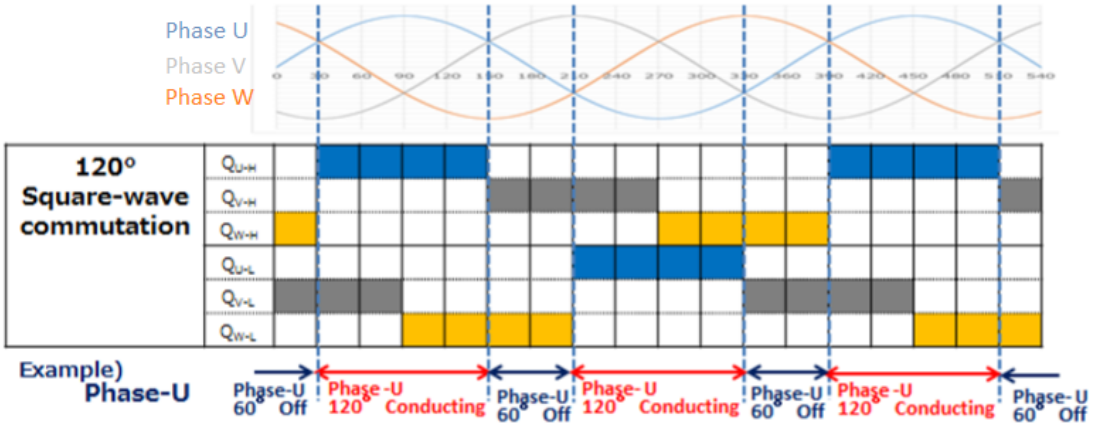

Figure 2.11. Switching of six devices for 120° square-wave commutation [17]

These 6-steps, or commutation phases, move an electromagnetic field which induces the permanent magnets of the rotor to move the motor shaft.

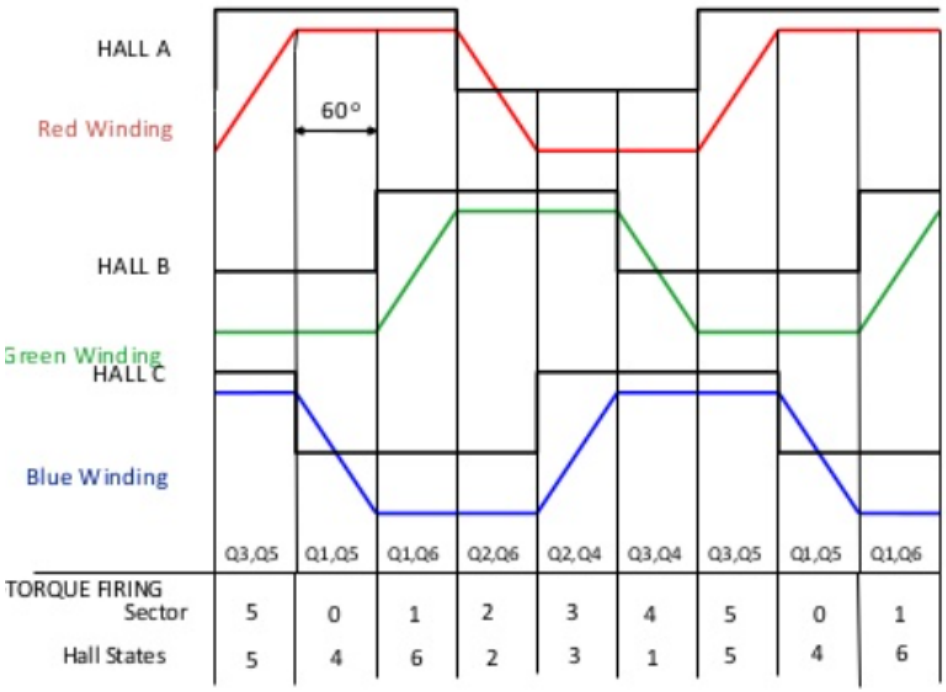

Figure 2.12. Six-step commutation based on three hall effect sensors [18]

Figure 2.12 illustrated commutation based on the three hall effect sensor values.

Since six-step control is a simple and easy way to drive motor, it has been commonly used in synchronous magnetic motor control. Six-step control already exists ten years ago. But for the low cost control system, it still being used for low precision control system. The system in this project does not require very high control precision and a certain torque ripple is acceptable, so it is reasonable to utilize six-step commutation. Six-step commutation is also referred to as 120° square-wave commutation [17] .

The easiest way to know the correct moment to commutate winding voltage is to obtain rotor positional feedback. Revolver, Optical Encoder and Hall Effect sensors are common motor position sensors. Many motor manufacturers supply motors with a three-element Hall effect position sensor because hall effect sensor is cheaper compare to others. Each sensor element outputs a digital high level signal for 180 electrical degrees of electrical rotation, and a low level for the other 180 electrical degrees. The three sensors are offset from each other by 120 electrical degrees so that each sensor output is in alignment with one of the electromagnetic circuits.

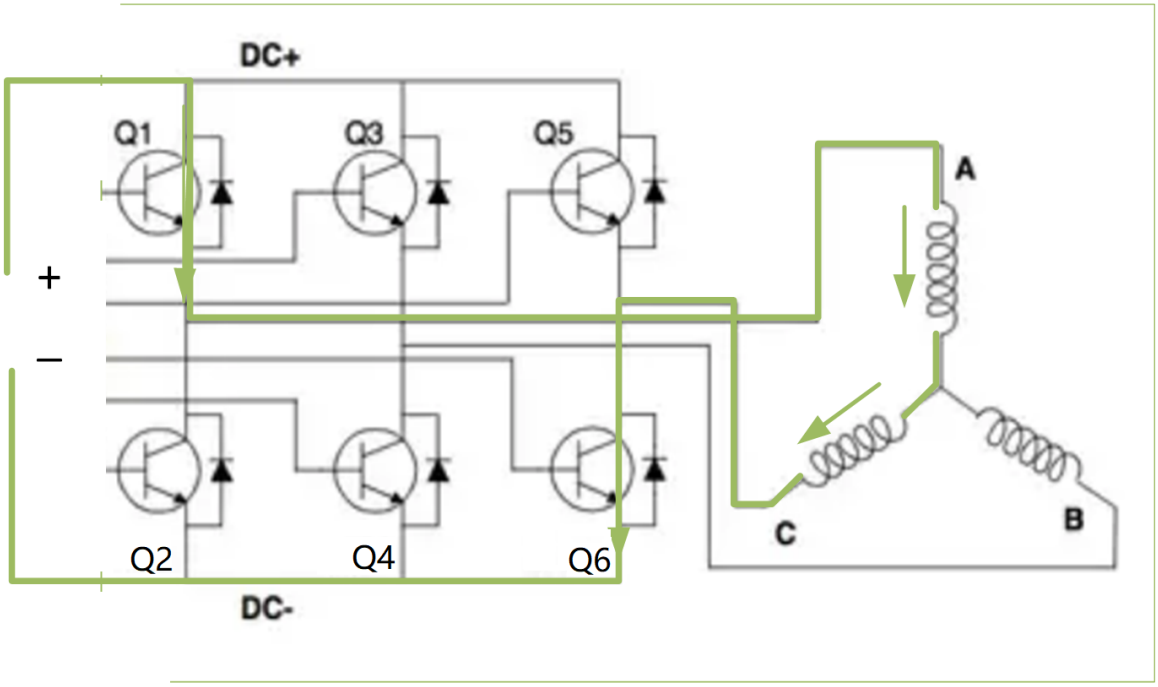

Figure 2.13. Motor control topology

In six-step control, each driving phase has one terminal driven to high, one motor terminal driven to low, while the third terminal is just kept floating. In Figure 2.13, Green line exhibits one step that current goes through Q1, phase A, phase C and Q6 by turning on high side Q1 and low side Q6. Changing the duty cycle of the PWM can change the voltage of the terminals. This control method is used to implement speed and current adjustment. There are different methods to set the PWM control method. For example, we can set high side of one phase as pulse width modulation and Low side of another phase "always on" instead of being modulated. Using this method, we can greatly reduce the switching loss of the MOSFETs.

Figure 2.13 showed how to use six-step square-wave commutation for a three-phase sinusoidal back emf motor. If the motor has Hall effect sensors installed, three Hall effect sensors output 2^3 different states. States 000 and 111 do not represent any correct rotor position. The six remaining states represent the normal states. Abnormal 000 and 111 states could happen when Hall effect sensors fail or when there is interference with the sensor signal. The six normal states decide are used to make commutation decisions. Table 2.2 shows how six-leg MOSFETs respond to the Hall effect sensor signals.

Table 2.2. Truth Table for Square Wave Commutation

Status	Ha	Hb	Hc	Q1	Q2	Q3	Q4	Q5	Q6
1	1	0	0	0	0	1	0	0	1
2	1	1	0	1	0	0	0	0	1
3	0	1	0	1	0	0	1	0	0
4	0	1	1	0	0	0	1	1	0
5	0	0	1	0	1	0	0	1	0
6	1	0	1	0	1	1	0	0	0

2.4.2 Sinusoidal Pulse Width Modulation Control

Six-step commutation control based on Hall effect position feedback was discussed in the last section. Obviously trapezoidal voltage leads to current and torque ripple because of the harmonic generation. Sinusoidal Pulse Width Modulation control (SPWM) can be used in PMSM, which reduces torque ripple and noise. Figure 2.14 illustrates generation of the Sinusoidal PWM and Figure 2.15 represents the SPWM result [19].

Figure 2.14. Sinusoidal PWM modeling

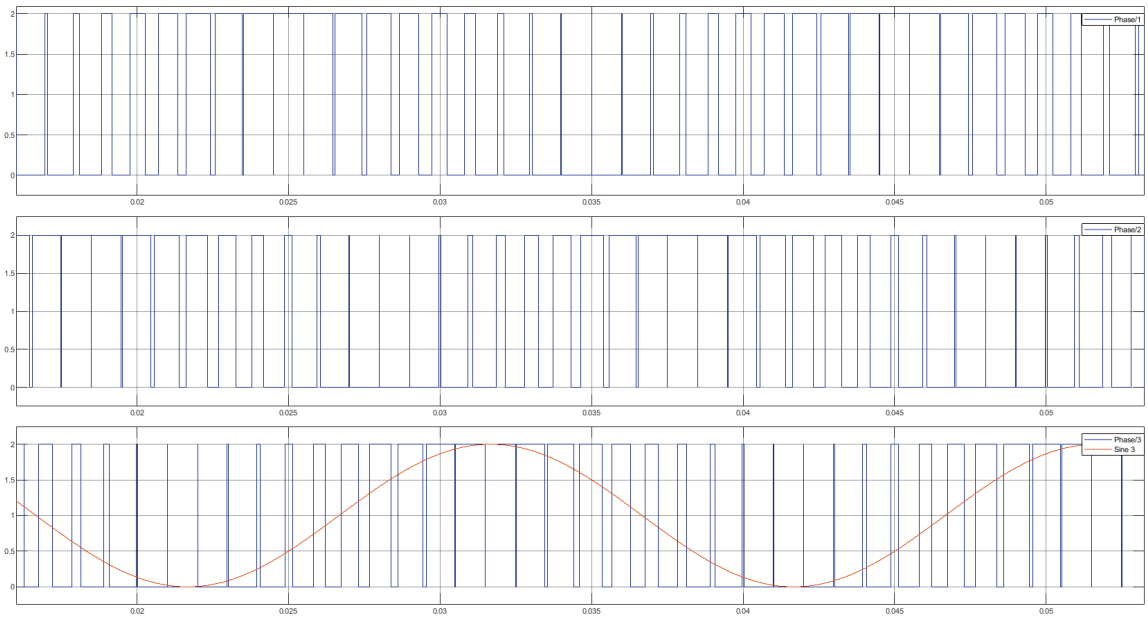

Figure 2.15. Sinusoidal PWM output

When modulating phase voltage, the maximum phase to phase voltage is:

$$V_{ref} = 2\sin\frac{\pi}{3}\frac{V_{DC}}{2} = 0.866V_{DC} \tag{2.7}$$

2.4.3 Space Vector Pulse Width Modulation Control

Reducing harmonic distortion and building a sinusoidal voltage for PMSM will increase the efficiency of the motor control. Space Vector Pulse Width Modulation(SVPWM) can generate sinusoidal wave, which can reduce torque ripple significantly. Compared to SPWM, it has less switching losses due to the switching strategy [20]. Equation 2.7 shows that SPWM can achieve 0.866Vdc, but SVPWM contributes full V_dc which means that it increases the Vdc utilization 15% more compared to SPWM control method.

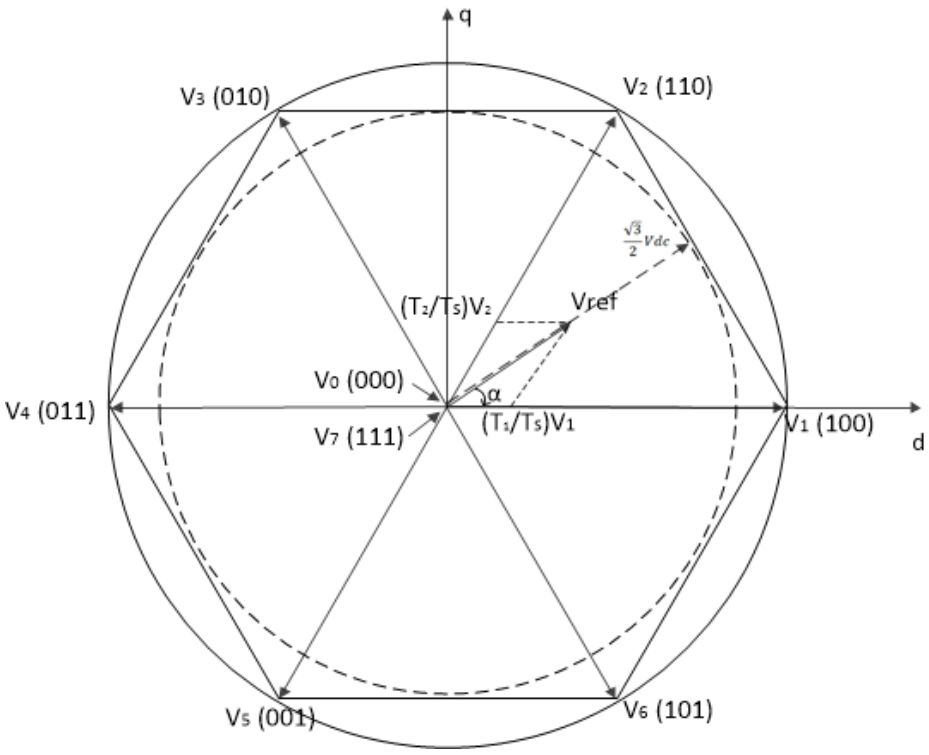

Figure 2.16. Sector based switching pattern of a space vector modulation.

The purpose of the SVPMW control is to generate a fixed amplitude flux and let the rotor always has a 90 degree angle to follow stator flux. As seen in Figure 2.16, Vref is a space reference vector which is what we want to get. The whole space is equally divided into six sectors. Each sector is bounded by two consecutive vectors. For example, sector 1 is surrounded by V2 and V1. By controlling the amplitude and

frequency of the Vref, we can achieve a certain motor voltage and the motor speed. Each vector represents the switching device status. For instance, vector V1 represents Q1, Q4, Q6 (shown as "100" showed in Table 2.3. This means that high side Q1, low side Q4 and Q6 are turned on. For getting the full amplitude of Vref vector, phase A contributes $\frac{2}{3}V_{dc}$ and the other phases contribute $-\frac{1}{3}V_{dc}$. There are eight possible switching vectors. V1 through V6 are six active switching vectors, while V0 and V7 are two zero vectors.

Table 2.3. Truth Table for Square Wave Commutation

Space Vector	Switching			Phase Voltage			Line Voltage		
V	A	B	C	V_{aN}	V_{bN}	V_{cN}	V_{ab}	V_{bc}	V_{ac}
V_0	0	0	0	0	0	0	0	0	0
V_1	1	0	0	$\frac{2}{3}V_{DC}$	$-\frac{1}{3}V_{DC}$	$-\frac{1}{3}V_{DC}$	1	0	-1
V_2	1	1	0	$\frac{1}{3}V_{DC}$	$\frac{1}{3}V_{DC}$	$-\frac{2}{3}V_{DC}$	0	1	-1
V_3	0	1	0	$-\frac{1}{3}V_{DC}$	$\frac{2}{3}V_{DC}$	$-\frac{1}{3}V_{DC}$	-1	1	0
V_4	0	1	1	$-\frac{2}{3}V_{DC}$	$\frac{1}{3}V_{DC}$	$\frac{1}{3}V_{DC}$	-1	0	1
V_5	0	0	1	$-\frac{1}{3}V_{DC}$	$-\frac{1}{3}V_{DC}$	$\frac{2}{3}V_{DC}$	0	-1	1
V_6	1	0	0	$\frac{1}{3}V_{DC}$	$-\frac{2}{3}V_{DC}$	$\frac{1}{3}V_{DC}$	1	-1	0
V_7	0	0	0	0	0	0	0	0	0

There are several different ways to implement the SVM control [21]. The most common way is conventional SVM. The relationship between the stator phase voltage and stationary frame d-q is showed in Equation 2.8.

$$\begin{bmatrix} V_d \\ V_q \end{bmatrix} = \frac{2}{3} \begin{bmatrix} 1 & -\frac{1}{2} & \frac{1}{2} \\ 0 & \frac{\sqrt{3}}{2} & -\frac{\sqrt{3}}{2} \end{bmatrix} \begin{bmatrix} V_{an} \\ V_{bn} \\ V_{cn} \end{bmatrix} \tag{2.8}$$

We also can get the amplitude of Vref and the rotor position from Equations 2.9 and 2.10.

$$| V_{ref} | = \sqrt{V_d^2 + V_q^2} \tag{2.9}$$

$$\alpha = \tanh \frac{V_q}{V_d} \tag{2.10}$$

SVM switching rules helps limit switching times and generate the maximum line to line voltage. SVM vector Vref is always tracking a circle. Each time only one switching switches when changing vector status and no more than three switchings are involved in one time Ts. When entering the next section, the previous final status should be the initial status in this new section. Table 2.4 explained the switching sequence following the above rules. Lower side Q2, Q4 and Q6 has complimentary signal corresponding to the high side. Figure 2.18 represents the SVM method of generating SVPWM in high side. The low side has the complimentary voltage signal corresponding to the high side. Using Equation 2.8, 2.9 and 2.10, we transfer 3-axis stator voltages to 2-axis d and q and also achieve angle and Vref. Six sectors have been generated by using the angle. Following the idea of [22] and [23], SVM simulation was built in MATLAB/SIMULINK. Figure 2.17 illustrates how to decide sector using angle. In Figure 2.18 , a MATLAB function has been used to transfer T1, T2 and T0 to three-phase voltage (Figure 2.19). Table 2.4 represents time distribution in Q1, Q3 and Q5.

Table 2.4. SVM Switching Table

Sector	Upper switches Q1,Q3,Q5
1	$S_1 = T_1 + T_2 + \frac{T_0}{2}$ $S_3 = T_2 + \frac{T_0}{2}$ $S_5 = \frac{T_0}{2}$
2	$S_1 = T_1 + \frac{T_0}{2}$ $S_3 = T_1 + T_2 + \frac{T_0}{2}$ $S_5 = \frac{T_0}{2}$
3	$S_1 = \frac{T_0}{2}$ $S_3 = T_1 + T_2 + \frac{T_0}{2}$ $S_5 = T_2 + \frac{T_0}{2}$
4	$S_1 = \frac{T_0}{2}$ $S_3 = T_1 + \frac{T_0}{2}$ $S_5 = T_1 + T_2 + \frac{T_0}{2}$
5	$S_1 = T_2 + \frac{T_0}{2}$ $S_3 = \frac{T_0}{2}$ $S_5 = T_1 + T_2 + \frac{T_0}{2}$
6	$S_1 = T_1 + T_2 + \frac{T_0}{2}$ $S_3 = \frac{T_0}{2}$ $S_5 = T_1 + \frac{T_0}{2}$

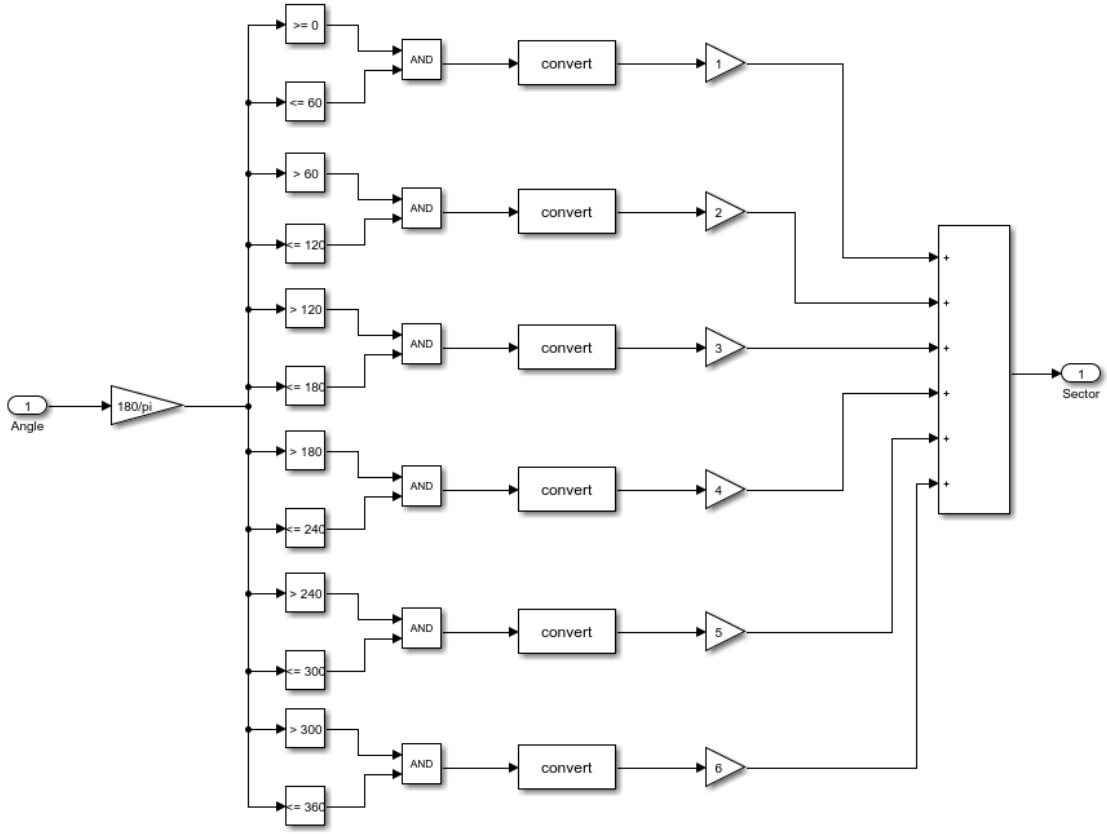

Figure 2.17. Relationship between angle and sector

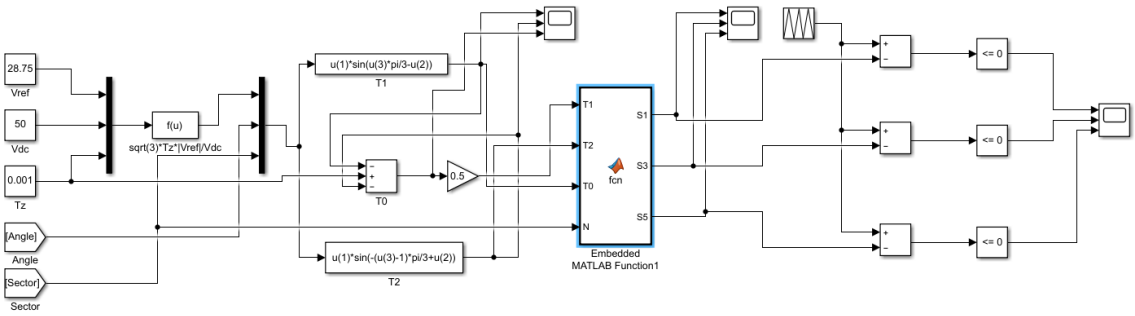

Figure 2.18. Space vector modulation simulation block

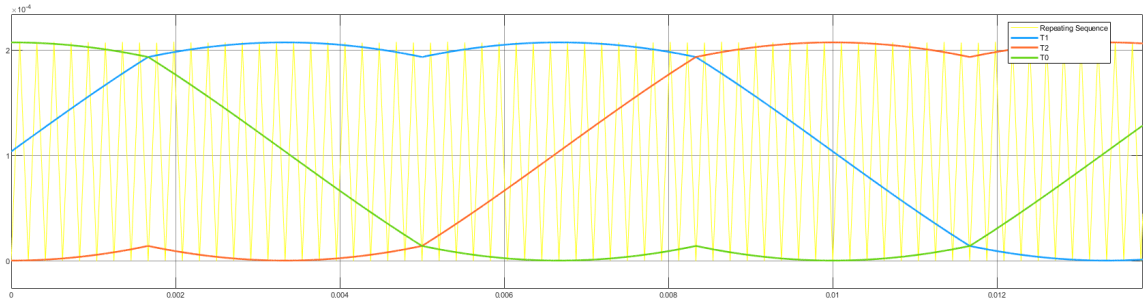

Figure 2.19. Saddle waveform on three-phase

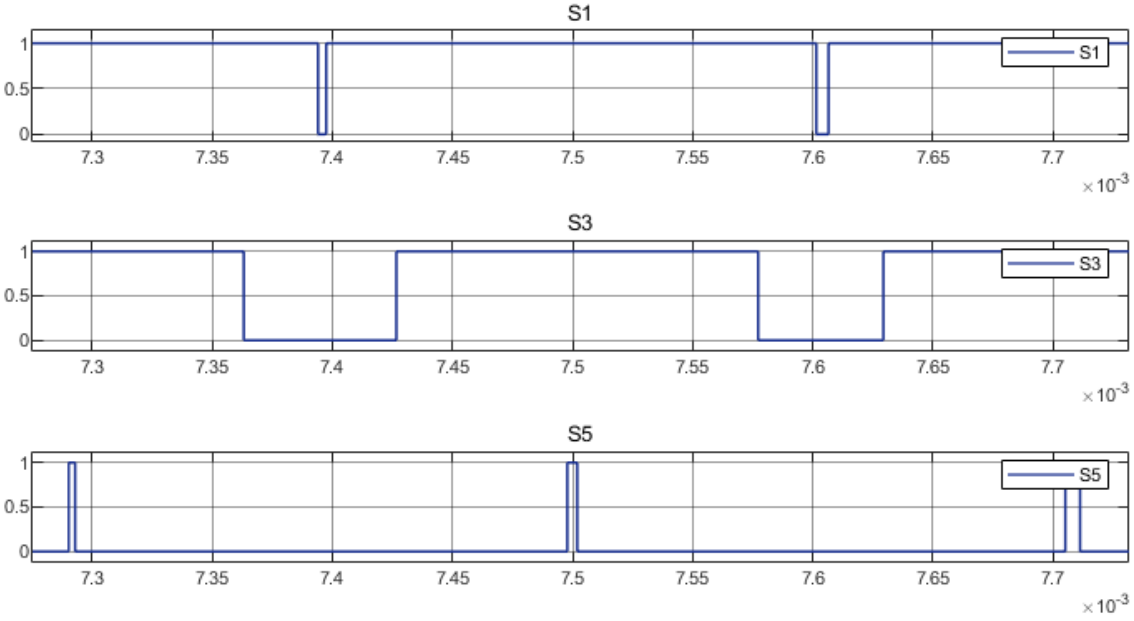

Figure 2.20. Space vector modulation generate PWM for high side

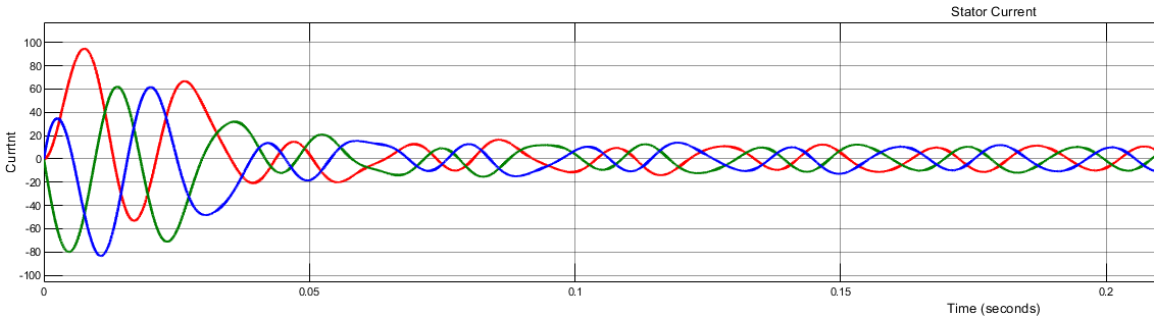

Figure 2.21. Three-phase current using SVPWM

As seen in Figure 2.19, a third harmonic component is injected on the fundamental waveform. This additional harmonic component comes from using inactive status which does not exist in SPWM. Thus, SVM could over modulate and get the full DC voltage, which means SVPWM could generate 15% more voltage compared to general SPWM. This has led to this method being commonly used. Figure 2.21 shows three-phase current. Compared to the current curve running in the six-step method (Figure 2.30), SVM is an efficient way to smooth current and has better performance.

2.4.4 Field Oriented Control

Field Oriented Control (FOC) is a type of vector control. If the load changes are frequent and unpredictable, six-step control is not suitable due to dynamic loading changing. FOC uses current feedback to control the torque of 3-phase motors and rotor magnetizing flux. Using SVM as discussed in the previous subsection, PMSM achieves a very smooth speed and torque. Combined with a high switching frequency three-phase bridge and a high speed microprocessor, FOC can be implemented in either hardware or software. Figure 2.22 shows how FOC works. Clarke transformation moves three-axis current samplings from the stator onto two-axis α and β. The next step is coordinate α-βaxis to rotor axis, d and q. Error signals are calculated using I_d and I_q and reference value for these two. Inverse Park transformation was used to transfer d-q axis back to α-β axis and then inverse Clarke transformation was used to get three modulated current by using SVM. [24]

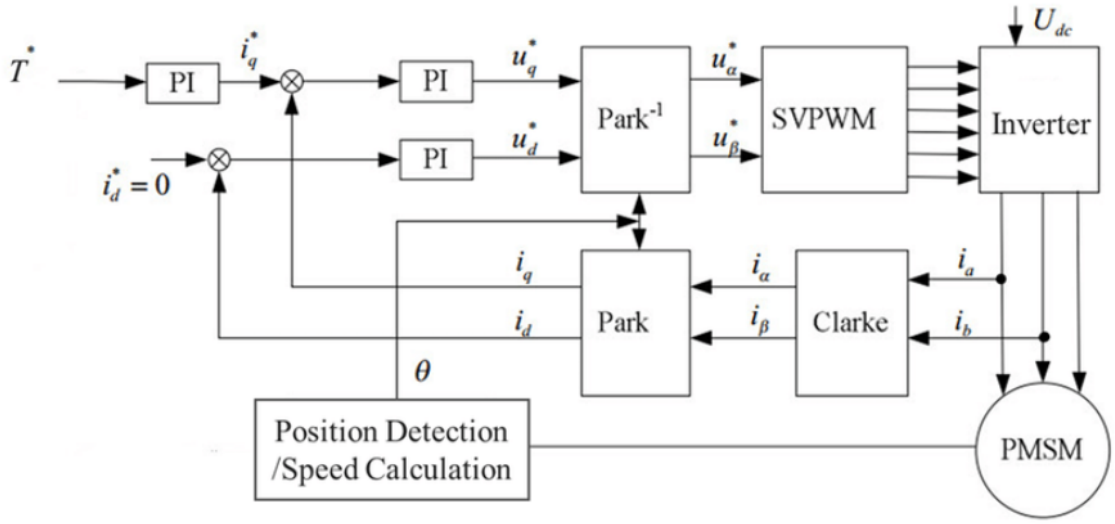

Figure 2.22. Block diagram of field oriented control [25]

As previously mentioned, this blade control system does not need high precision control. In most situations, the system stays in a constant speed with a speed difference range of ± 100 rpm. FOC is considered using in wheel control but for not this blade control system.

2.5 Grass Modeling

As discussed in Chapter 1, three key features will be considered: the height of the grass, the type of grass, and the proportion of dry and wet grass. To achieve better control performance, a study about the color and features of the grass was conducted by TASI (Transportation Active Safey Insitute) at IUPUI (Indiana University-Purdue University, Indianapolis). This study involved three steps: 1) generating the grass date set which could represent the grass distribution in the U.S., 2) defining the grass features, and 3) determining the representative color and height.

2.5.1 Grass Data Set

Google Street View was used to sample the grass in the U.S. (including Hawaii and Alaska). Firstly, 820,000 road locations were randomly sampled. Then, a stratified sub-sampling was conducted to balance the distribution bias including road levels, geographic location and population densities. As a result, 24,762 stratified locations with street view images were generated. To avoid effect of the brightness, images not in daylight, not in good weather, or under shade were eliminated from the sample set. Finally, 901 images were used to represent the grass in the U.S. The distribution of these 901 locations is shown in Figure 2.23. The locations cover all states in the U.S. Thus, we considered these 901 images as the representative of grass in the U.S.

2.5.2 Definitions of Grass Features

A study was conducted by TASI to find the grass features [12]. In this study, four parameters are used to describe the features of grass. They are height, color, height evenness, and color evenness. Furthermore, the study found that the height evenness and color evenness are closely correlated.

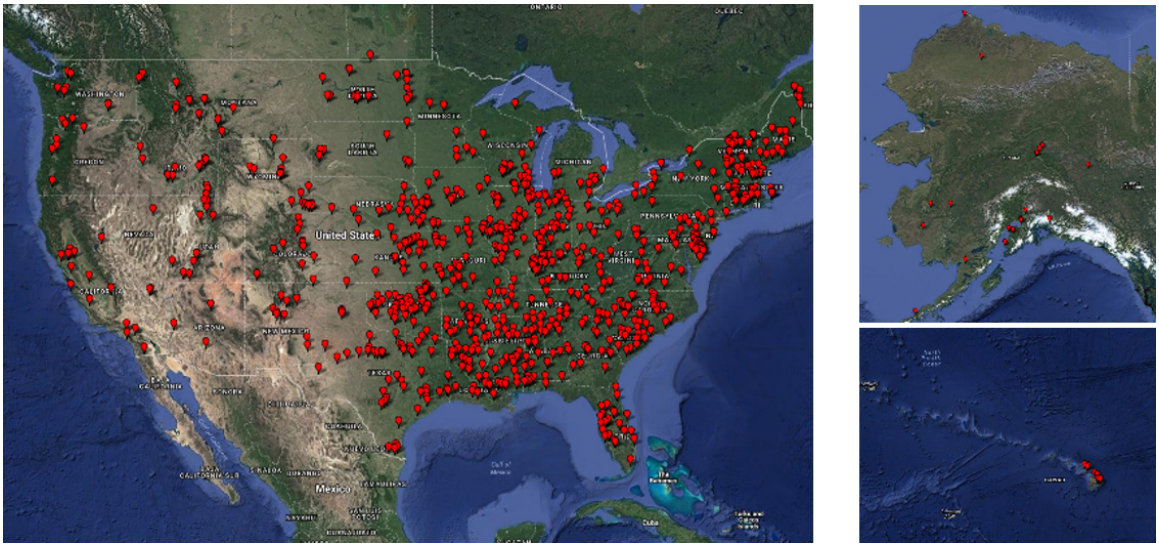

Figure 2.23. The distributions of abstracted grass locations

2.5.3 The Methodology for Grass Feature Determination

Height and height evenness of the grass were determined by manual clicking with the referencing of gathered images with known grass height and height evenness. The results showed that the short grass (2-5 inches) is the most common grass type with 68.6% of all sampled images, the medium grass (6-10 inches) is less than short grass, but still owns 28.9%. The proportion of tall grass (greater than 10 inches) only cover 2.5%.

To determine the grass color and height/color evenness, a k-means clustering was performed in the LUV color space. Six different colors with three levels of brown/yellow color and three levels of green color were obtained (Shown in Figure 2.24). For more details about the determination of the grass colors and color/height evenness, please refer to [12]. The methodology was shown in Figure 2.25.

Color	**Yellow**			**Green**		
						
RGB	111 95 65	146 130 96	170 162 135	99 100 55	105 110 44	139 141 87
LUV	41.130 11.889 22.194	54.991 12.107 25.976	66.624 6.377 21.007	41.284 1.491 29.380	44.713 -0.368 39.650	57.296 1.393 36.831
Marker	**5**	**1**	**6**	**2**	**4**	**3**
Locations	108	222	149	193	124	218

Figure 2.24. The representative colors

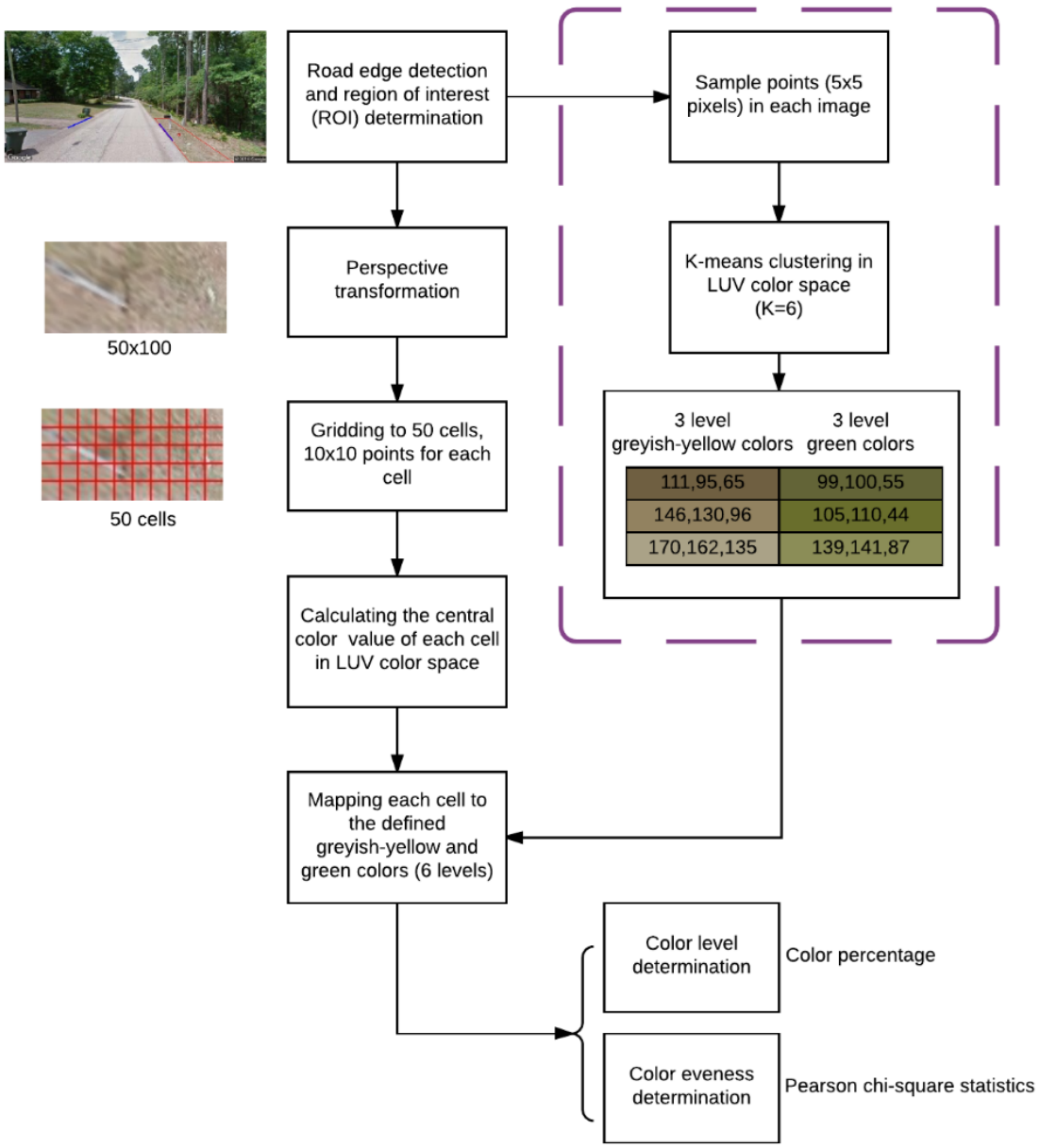

Figure 2.25. The methodology for grass feature determination

As mentioned in Section 2.5.2, the color evenness and height evenness are closely correlated. Thus, the grass was modeled as the portion of the six levels of yellow and green colors referring to the portion of wet and dry grass. When simulated, the grass was treated as the torque load. It was described as follows.

$$T_{grass} = \sum_{i}^{6} a_i c_i \tag{2.11}$$

where, i=1 to 6, means 6 levels of color,

a_i is the torque constant of the i-th color,

c_i is the portion of the i-th color.

2.6 Dynamic Mathematical Model

Through this standard motor commutation sequence, the motor controller generates a high frequency pulse-width modulated (PWM) signal to effectively reduce the average voltage and consequently change motor speed. The DC voltage source can even be significantly higher than the rated voltage of the motor. Thus, a wide range of motors can be used in the design. For maintaining accurate control of the motor, rotor position feedback θ is achieved for the commutation of the motor. As an example, a six-step control model was built in MATLAB/SIMULINK (shown in Figure 2.26). This is a closed-loop speed control system. A PID anti-winding controller was built to control the speed precisely. It continuously calculates the error between the output speed and the reference speed and adjusts the speed quickly. MATLAB is a very powerful mathematical tool that has plentiful libraries we can use directly. In this model diagram, ia PMSM/BLDC motor model from Universal Bridge is used to simulate a three-phase bridge.

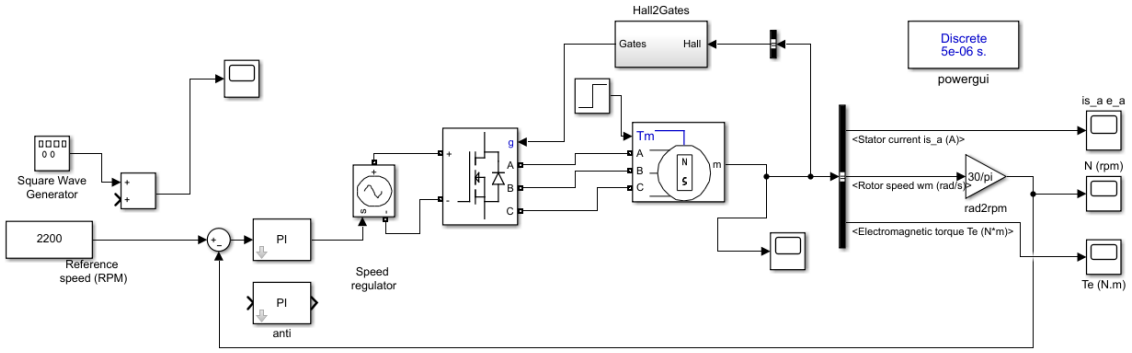

Figure 2.26. High power deck control system simulation

The motor specification settings are the following: Actuator like the motor can

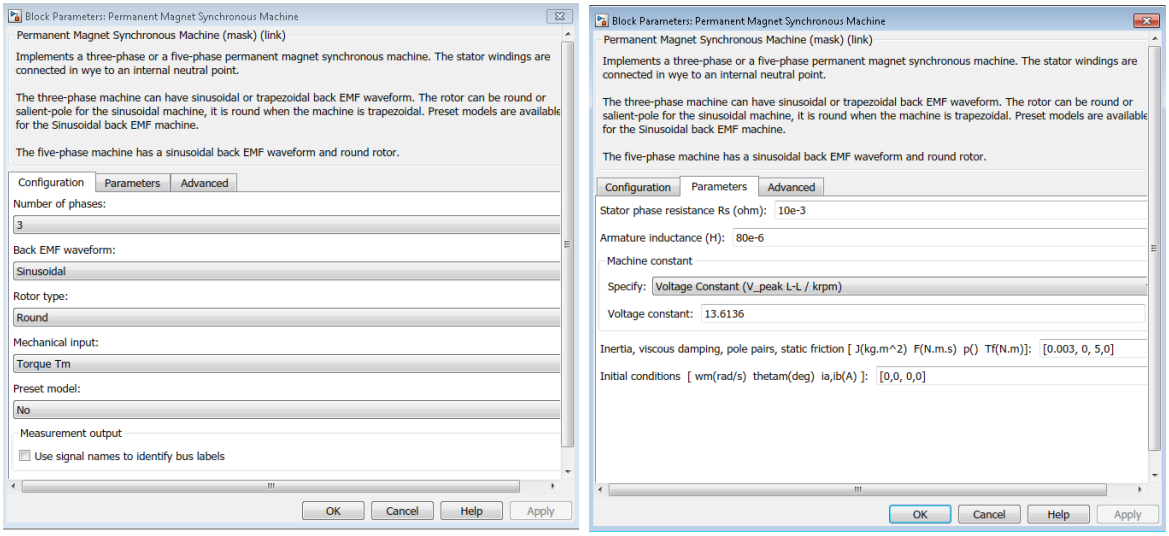

Figure 2.27. PMSM specifications

not respond to inputs at any ranges. It goes into saturation when receiving a large input. Anti-windup is commonly added in the PI controller.

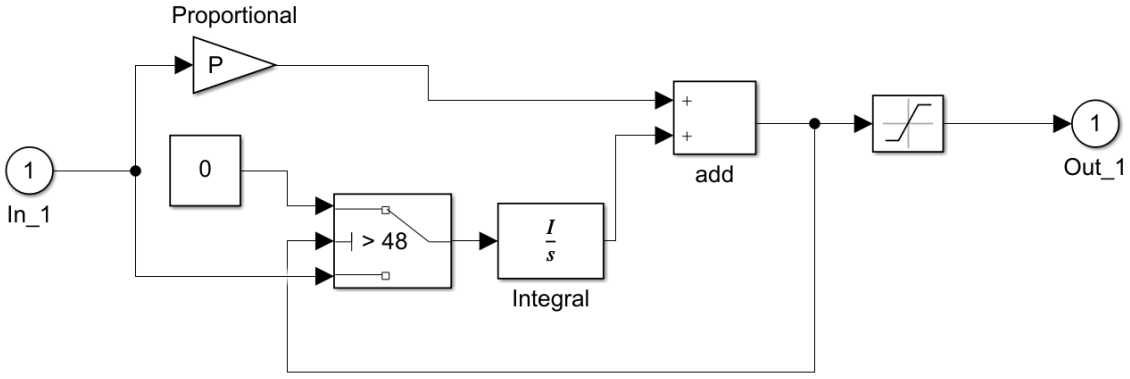

Figure 2.28. Anti windup PI controller

2.7 Simulation

Six-step closed-loop control was simulated in MATLAB/SIMULINK (Figure 2.26). Reference speed was varied from 2000 to 3000 RPM to simulate speed response. The error between reference speed and feedback speed was generated as PI controller input. Considering saturation in the real system, PI anti windup control was also designed. Figure 2.29 shows the result of setting 3000 RPM speed and adding 5 Nm Torque at 0.5s time. As seen in the figure, the speed reaches the 3000 RPM target in a short time. However, due to the six-step control which is not a circular space vector control, current and torque ripple obviously exist shown in Figures 2.30 and 2.31.

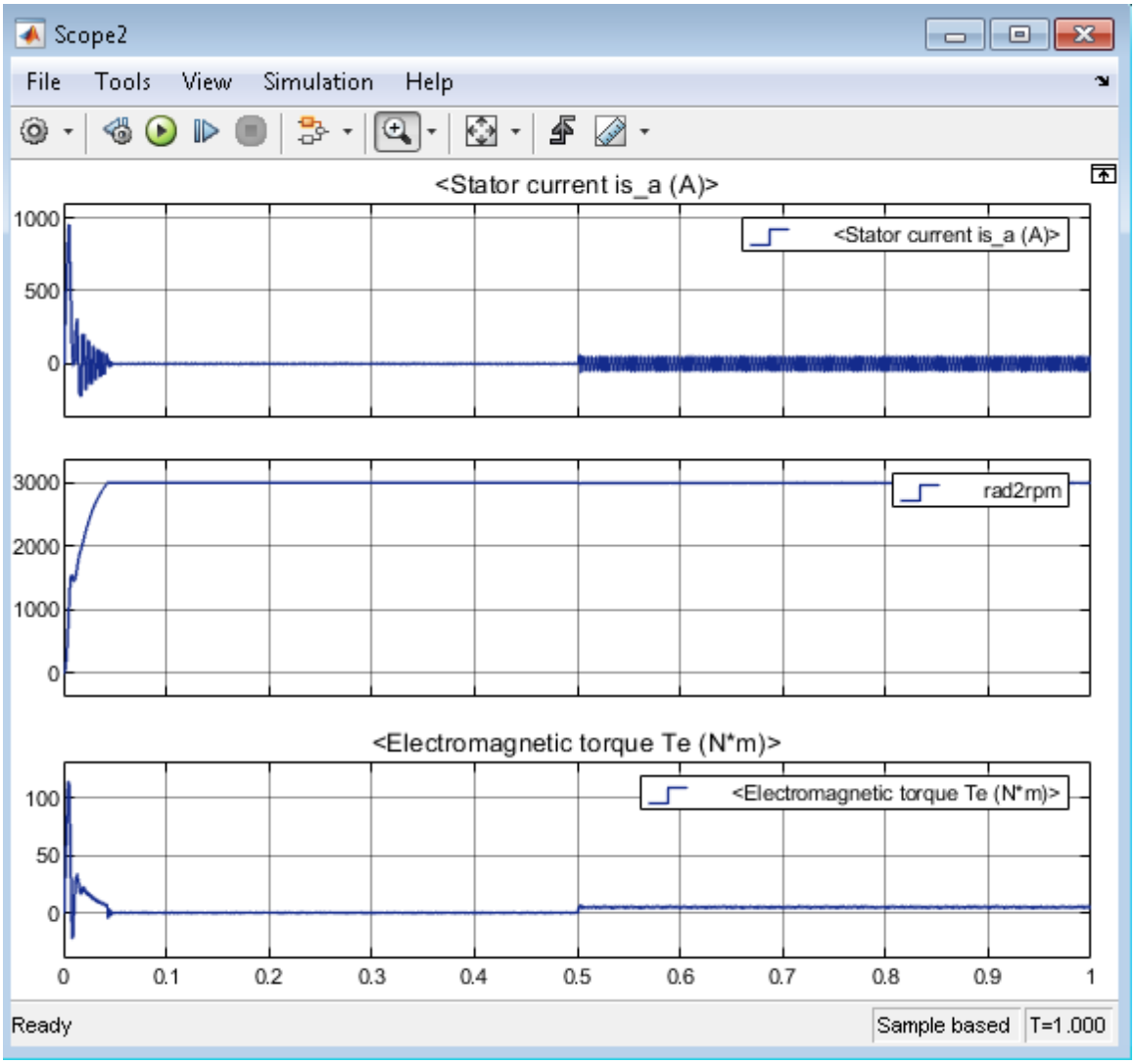

Figure 2.29. Simulation result of phase current, speed and torque

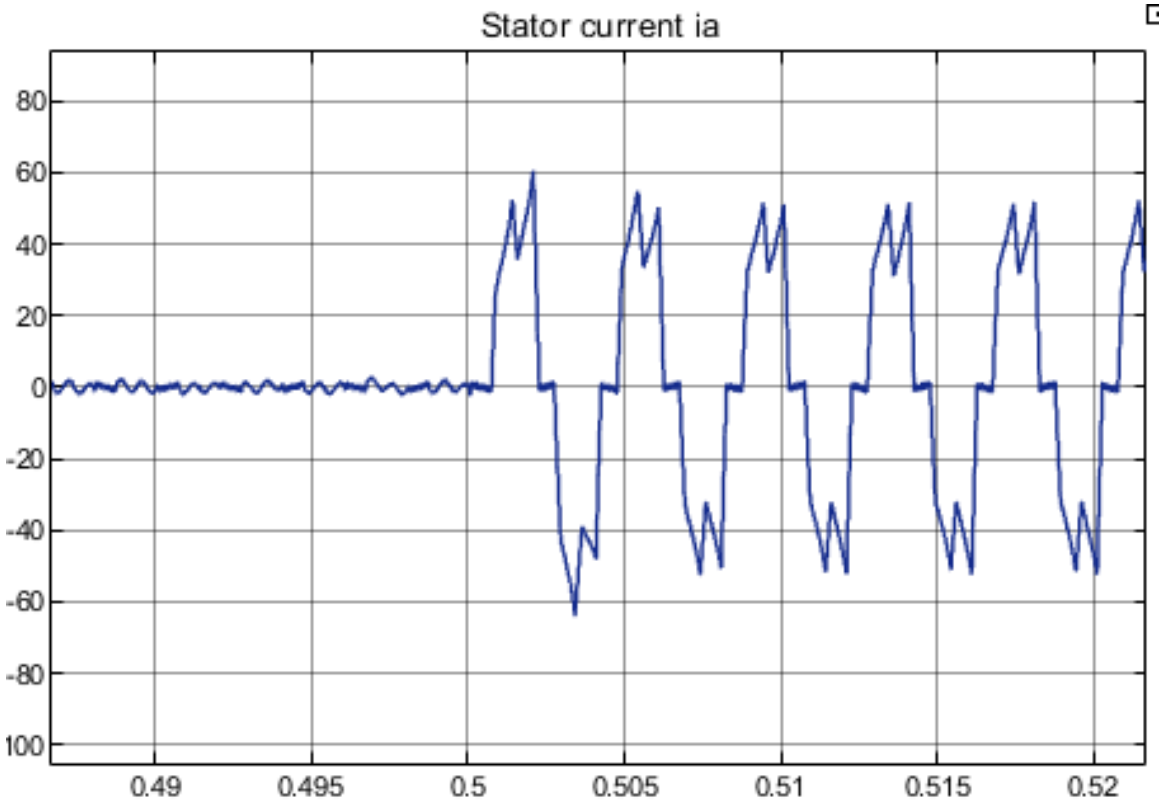

Figure 2.30. Enlarge phase current simulation

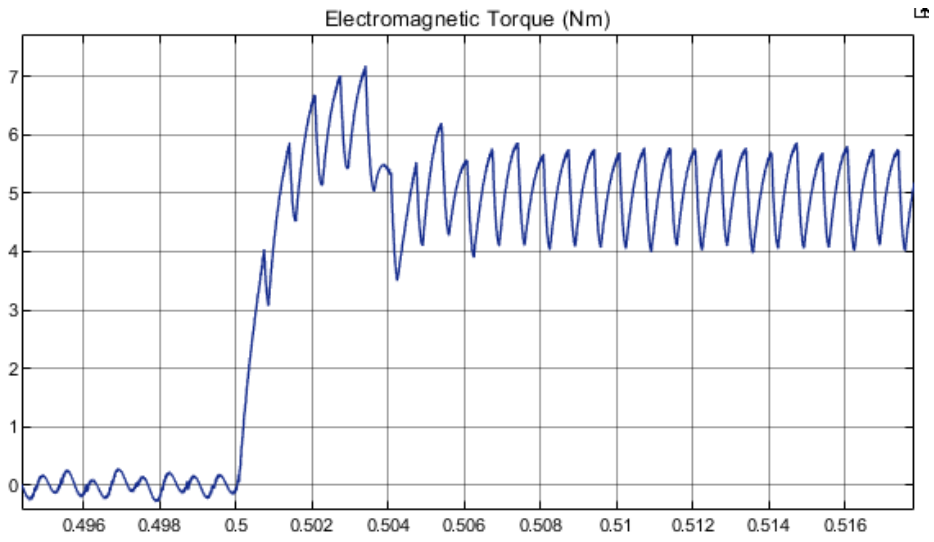

Figure 2.31. Enlarge torque output simulation

The anti-windup PI controller was introduced in the previous section. Figures 2.32 and 2.33 illustrate the simulation results of adding the anti-windup PI method.

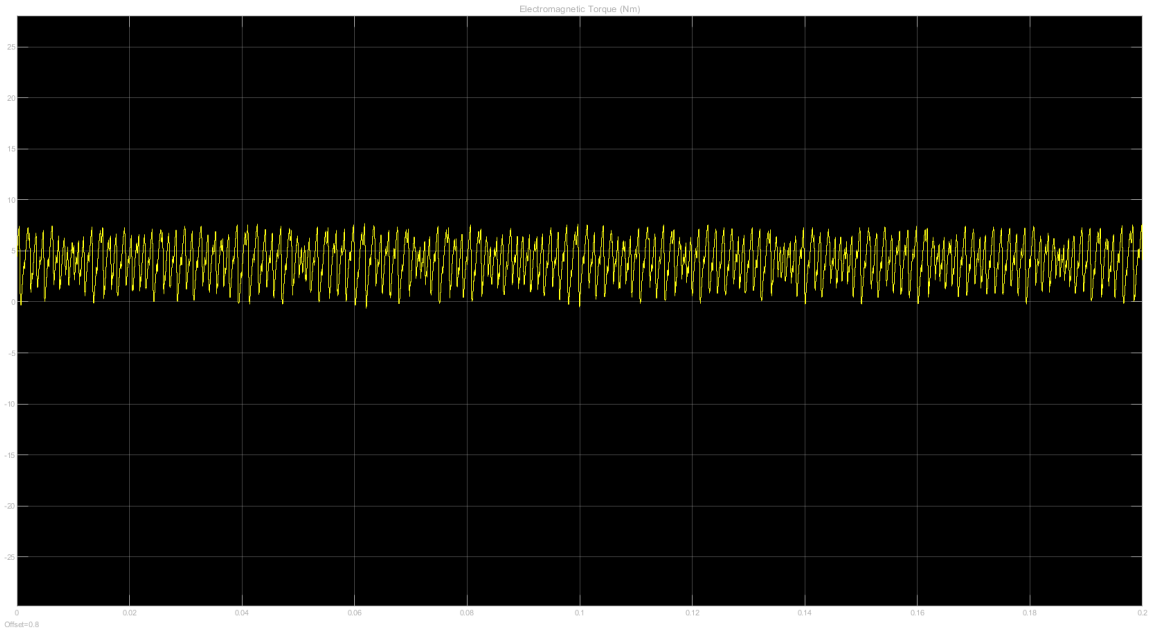

Figure 2.32. Anti windup torque simulation

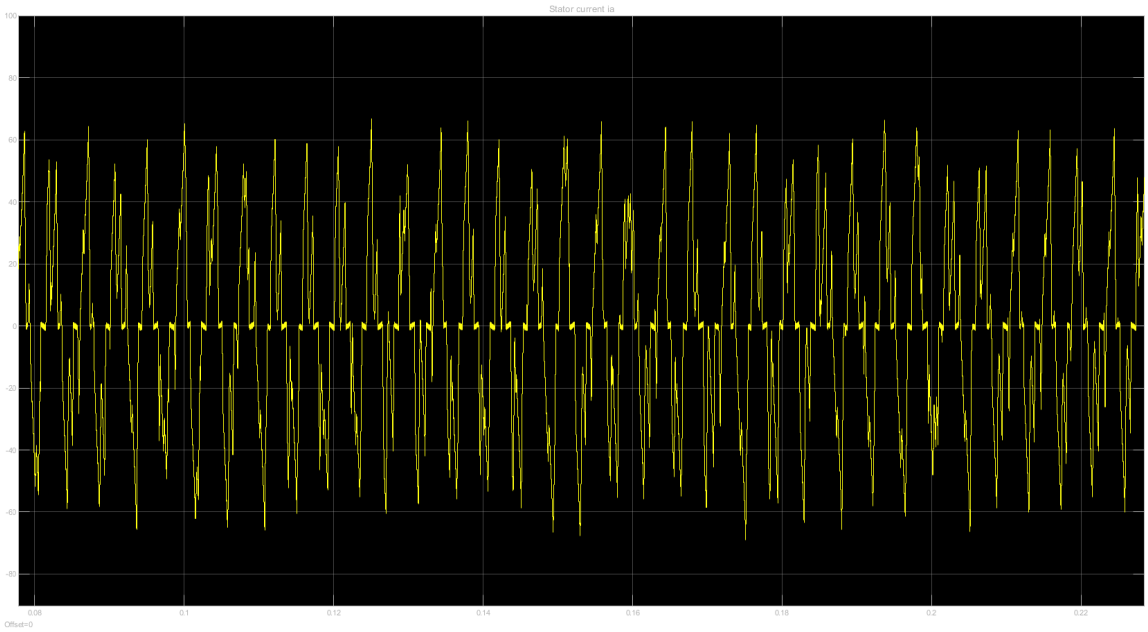

Figure 2.33. Anti windup current simulation

3. CONTROL SYSTEM HARDWARE DESIGN

The purpose of the high power deck control system is to control the three-phase permanent magnet synchronous motor. There are two popular control methods, which are 1) six-step control and 2) field oriented control. In order to reduce the cost and also to simplify the control algorithm, the former method was chosen. As shown in Figure 3.1, the main parts of the control system includes power management, Central processing unit(embedded processor), gate driving unit, three-phase inverter, Hall effect sensors(for position detection) and actuator.

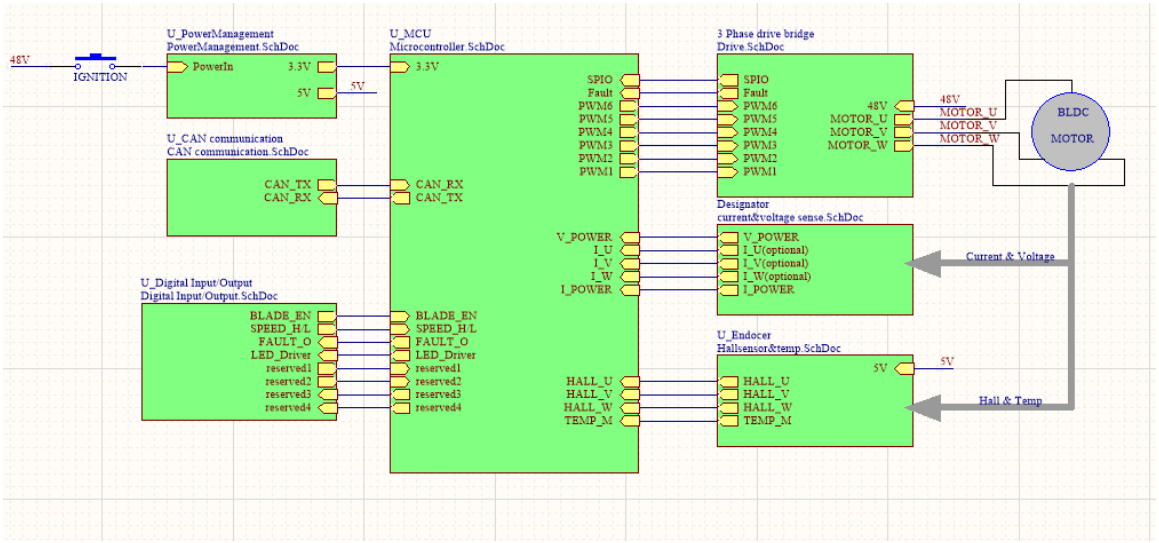

Figure 3.1. Block diagram of hardware schematic design

3.1 PMSM

A permanent magnetic synchronous motor has been used in this system.The stator is distributed winding with skewed teeth.Hence BEMF waveform of the stator is sinusoidal.Three phases is made up with a "Y" shape.The rotor includes eight

pole pairs permenant magnets(neodyium-boron-iron magnets).Three hall effect sensors were distributed in every 120 electrical degree inside and provide the position angle of the rotor. The temperature sensor was attached to stator windings to prevent over temperature. PMSM is the best candidate for this project due to very nice features such as the smaller size, higher power density, higher speed and smaller torque ripple and higher efficiency [26].

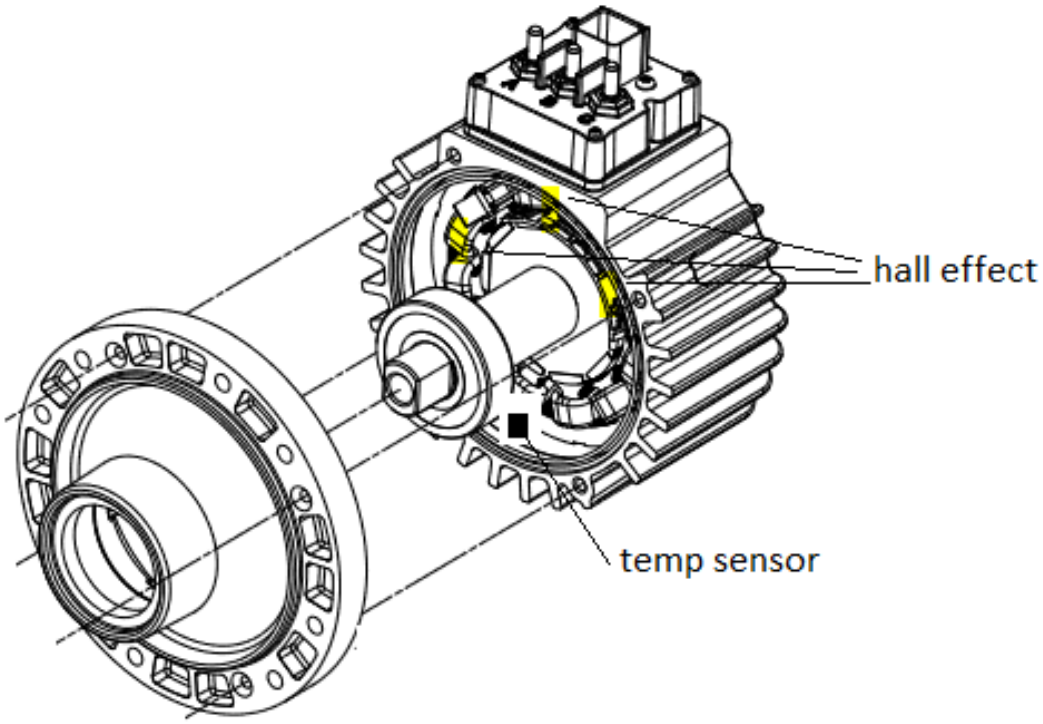

Figure 3.2. Permanent magnetic synchronous motor with position sensor and temperature sensor

3.2 Power Management

Power management plays an important roles in the whole system. The system cannot work properly without an stable power resource. In this electric mower system, four groups of 12 V lead-acid battery are used, which means that the battery provides

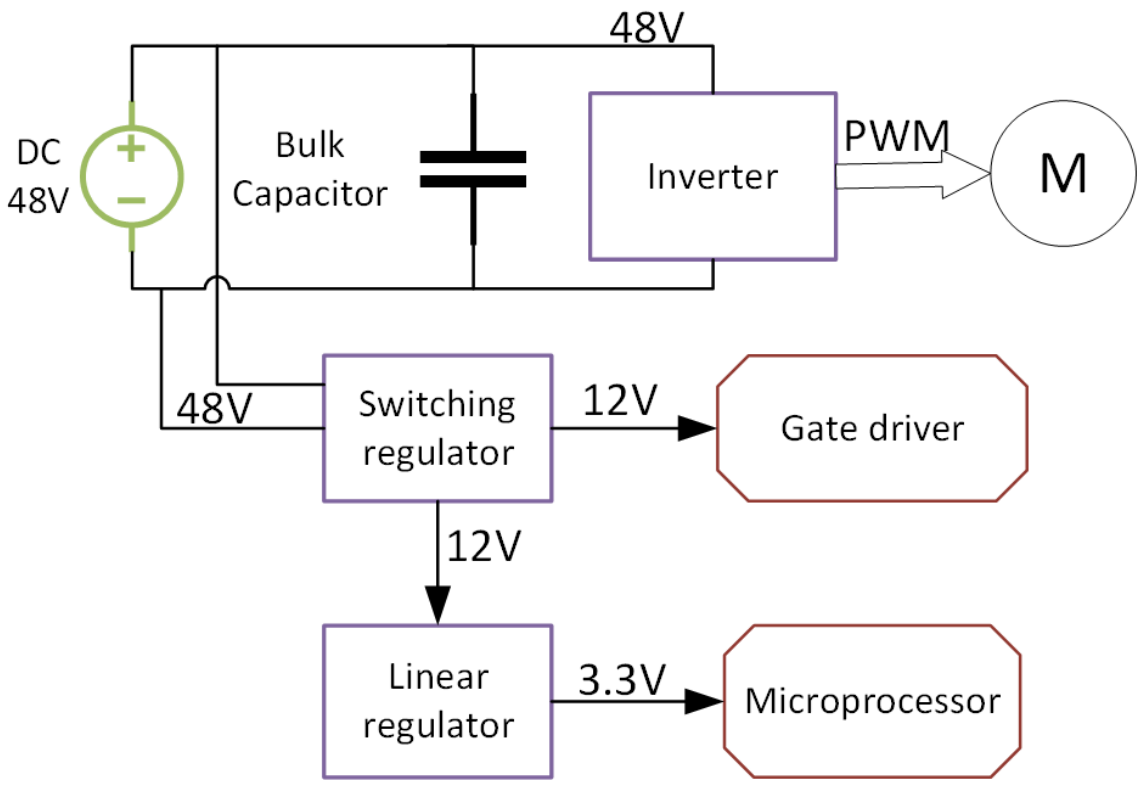

Figure 3.3. Power management of control system

48V DC power to the control system. The voltage range can be 42 V to 55V depending on the charging status. The gate driving unit needs 12V.The central control unit and OP AMP circuits need 3.3 V power. According to these requirements, the whole system power can be managed to three different voltage levels (Figure 3.3).

Considering the battery power range, a switching regulator, TPS54260, was selected. It is a 60-V, 2.5-A, step-down regulator with an integrated high-side MOSFET. The advantage of the switching regulation is high efficiency which can be more than 85%. The output voltage is set with resistor dividers and feedback to VSENSE pin 7 (Figure 3.4). Resistors with 1% tolerance or better are used here for achieving high precision results.

$$V_{out} = 0.8(R_{71} + R_{72})/R_{72} \tag{3.1}$$

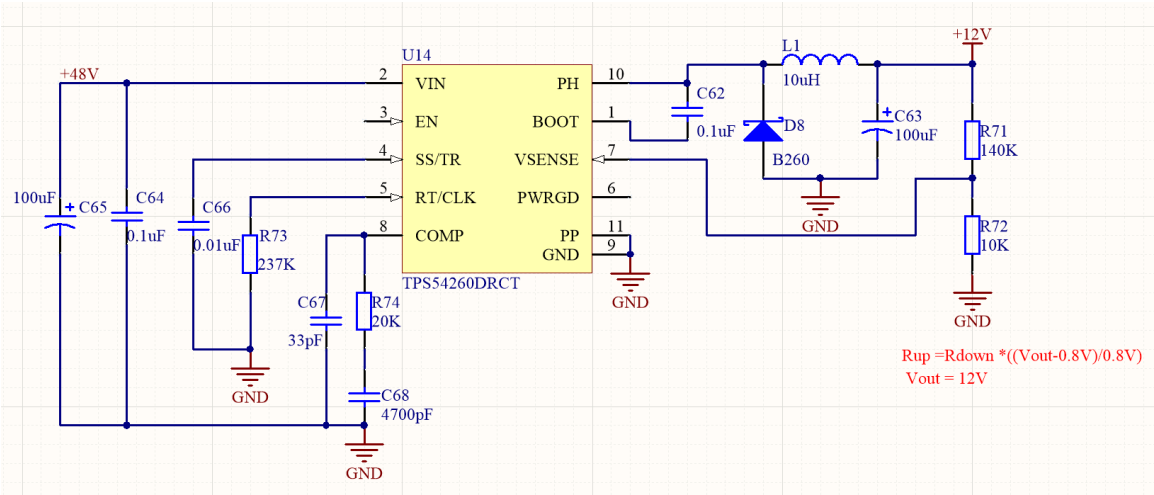

Figure 3.4. Switching regulate circuit converting 48V to 12V

In order to minimize the ripple on DC output which provides power to the microprocessor, linear regulator TLV1117 was used to generate the needed 3.3 V. This chip also minimizes the peripheral components, which only needs coupling capacitors. The disadvantage of the linear regulator is its lack of efficiency. A thermal dissipation pad had to be designed on the board.

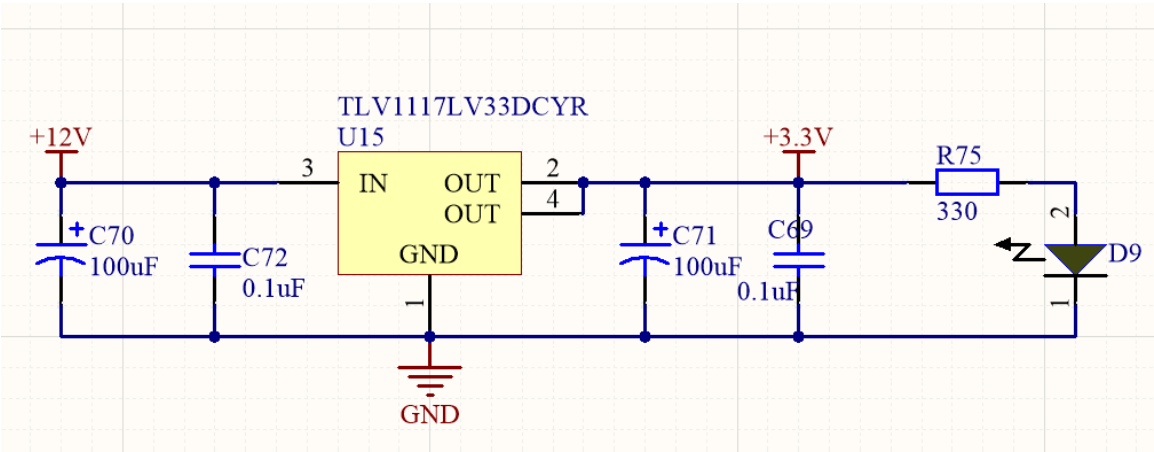

Figure 3.5. Linear regulate circuit converting 12V to 3.3v

3.3 Three-phase Inverter

In order to provide a proper current to three-phase motor, a power switching electronics device was used as an inverter. It can transfer DC power to alternate voltage to control the three-phase synchronous motor.

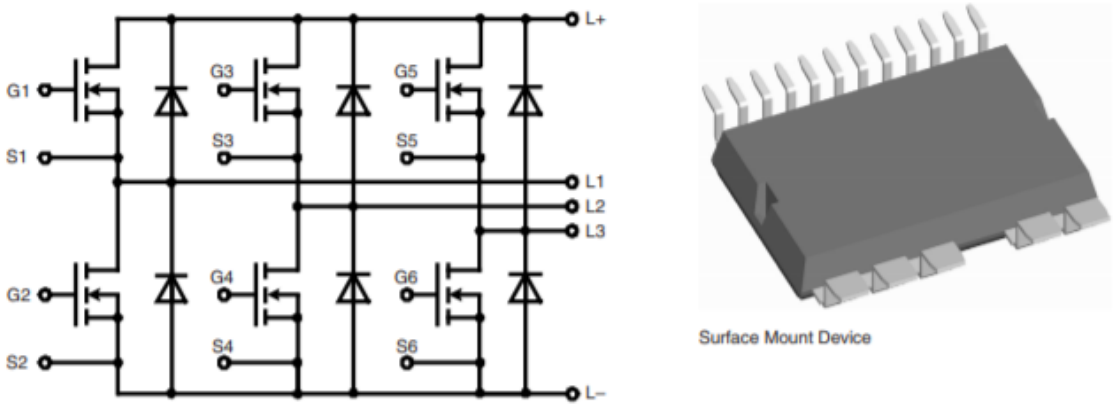

Figure 3.6. Integrated three-phase bridge [27]

The greatest advantage of using an inverter to drive a motor is that it can change the phase and frequency of motor drive currents according to the rotor position and therefore provides high drive efficiency and smooth motor rotation with little vibration at low to high RPM.

The three-phase full bridge inverter includes the six switching device shown in Figure 3.6. There are several different types of switching power device such as insulated-gate bipolar transistor(IGBT), MOSFET and transistor. MOSFET and IGBT are widely used as inverterS for motor control, due to their flexibility to arbitrarily control the output voltage or frequency.

IGBT can be used in high power field but has low switching frequency. MOSFET is very prevalent in small or middle power applications because it has low R_{DSon} and higher frequency. Considering switching noise in certain area, MOSFET switching frequency can be setup at up to 100 kHz, which can be very helpful in reducing noise.

Therefore, MOSFET was chosen for the three-phase switching bridge for this control system. In order to achieve a smaller size, an integrated power module has been used in this control system. This module integrates six N-channel MOSFETs in one package and has the benefits of saving space and size [27]. It also has an isolated base,so there is no need for additional isolation between the MOSFETs and the heat sink.

3.4 Position Feedback

In order to control the motor more precisely, it is necessary to add rotor position sensors. There are several ways to add position sensor such as Hall effect position sensor, quadrant encoder, and revolver. Considering the cost and assembly complexity, Hall effect sensors were utilized in this project. The RC filtering plays a key role in obtaining the rotor position. The motor will not receive a correct commutating sequence if Hall effect signals get disturbed. Figure 3.7 illustrates the obtaining one Hall effect signal, which also goes through a non-inverting buffer to enhance output performance.

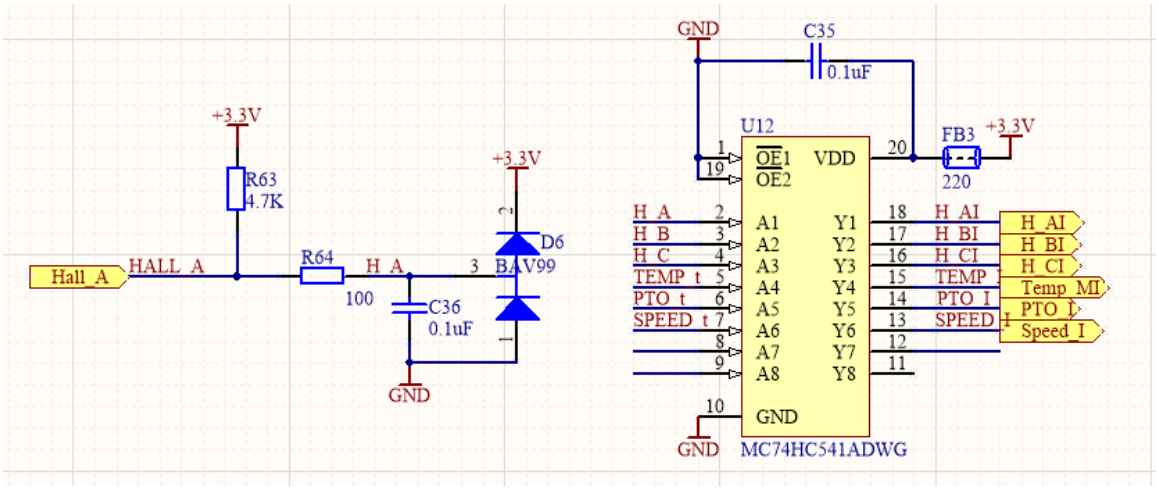

Figure 3.7. Hall effect position feedback circuit

Sensorless control can also be used in position detection. The advantage of sensorless control is the elimination of the Hall effect sensors and associated connections and circuits, which leads to hardware cost savings. Sensorless control will be considered in the next version.

Speed closed-loop control can be implemented by adding PID control in the front control path and calculating the error between reference speed and the feedback speed. In this way, the blade speed is stabilized in 3500 rpm± 100 rpm.

The Hall effect sensors can only provide the angular position within each electrical cycle. When the motor is running at a low speed, this obviously increases the torque ripple because of the commutation. If higher speed resolution is needed and cost is not a consideration, optical encoders and the resolver can be considered to mitigate this issue.

3.5 System Current Sensing

Over-current detection must be implemented in this control system. That means current sensing circuit has to be designed. In Figure 3.8 , shunt resistor R13 transferred current to voltage. Current Amplifier INA240 was used for accurate current measurements without large transients and associated recovery ripple on the output voltage [28].

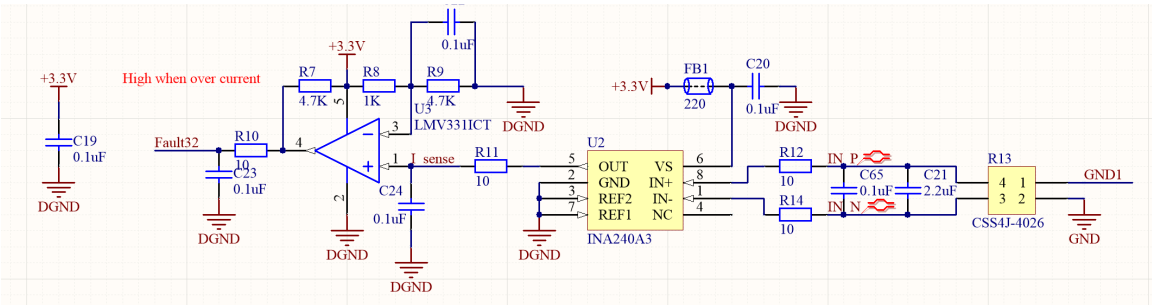

Figure 3.8. Current sensing circuit

3.6 Gate Driver Design

The microprocessor provides six PWM channels to change voltage on three-phase terminals, but these PWM signals cannot generate enough voltage to drive the MOSFETs directly. Typically most MOSFETs need a 10 V differential between gate and source. Three gate drivers need to be added between micro controller and MOSFET to provide stronger driving capability. Three gate drivers are used to drive the three-phase full-bridge inverter. Highly integrated gate drive DRV8303(Texas Instruments, Dallas, TX) integrates three independent half-bridge drivers. It includes a charge pump to generate the high side voltage. Each driver drives two N-channel MOSFETs (showed in Figure 3.9). There are extra functions also added in this gate driver, such as over-current detection and SPI based configuration. Hence, not only does the highly integrated gate driver decrease system component count, cost, and complexity, but it also takes over a lot of work from the processor.

Calculating the gate current during switching is necessary to verify the gate drive output capability. The gate current is calculated using equation 3.2, where Q is the gate charge in Coulomb (nC from the data sheet) and t is the switching time (in ns if using nC).

$$I_g = \frac{Q}{t} \tag{3.2}$$

The MOSFET switching time is in 5 0us, and a typical MOSFET with a total gate charge of 117 nC will need 2 mA. In terms of current calculation, this integrated driver satisfies the current requirement.

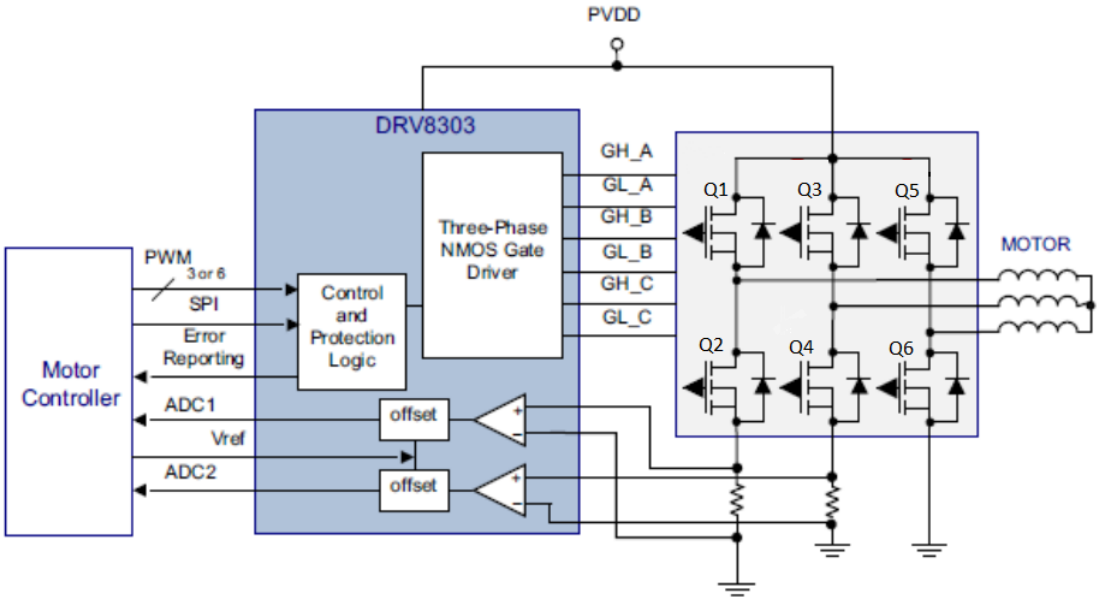

Figure 3.9. DRV8303 in block diagram of the control system

4. CONTROL SYSTEM SOFTWARE DESIGN

The firmware is developed using dsPIC33EP (Microchip Technology Inc., Chandler, AZ) and implements closed-loop speed control using a six-step algorithm. SVM control will be the next step to implement low ripple, high efficiency control. The whole program comes with various control and protection functions, such as overvoltage protection, overcurrent protection, over temperature protection and communicating with computer.

The software architecture of the control system is built in transitions of the six states shown in Figure 4.1. When the system gets power or is reset, it stays in static status and is ready to transfer to another state. When the turn on blade command is received, the system jumps into start up (speed acceleration). When speed goes into the range of target speed, state changes from start up to run. When stop command is received, system change it to stopping state and execute five second stopping function. After speed becomes zero, state transits to stop state. If any abnormal event happens, such as over current, over temperature and so on, system falls into fault state and logs the fault code.

4.1 Embedded System Design

The high power deck control system software includes embedded system programming and user interface programming. Microchip's dsPIC33EP 'MC' family offers 70 MIPS performance, a Digital Signal Processing (DSP) engine and specialized peripherals that can be used to implement high-efficiency, high-precision, variable-speed, constant-torque Proportional Integral (PI) control and Field Oriented Control (FOC) of motors. For the deck control system, dsPIC33EP128MC506 was chosen. The 7.14 ns PWM resolution is very beneficial for 6 channel inverter control and its ability to

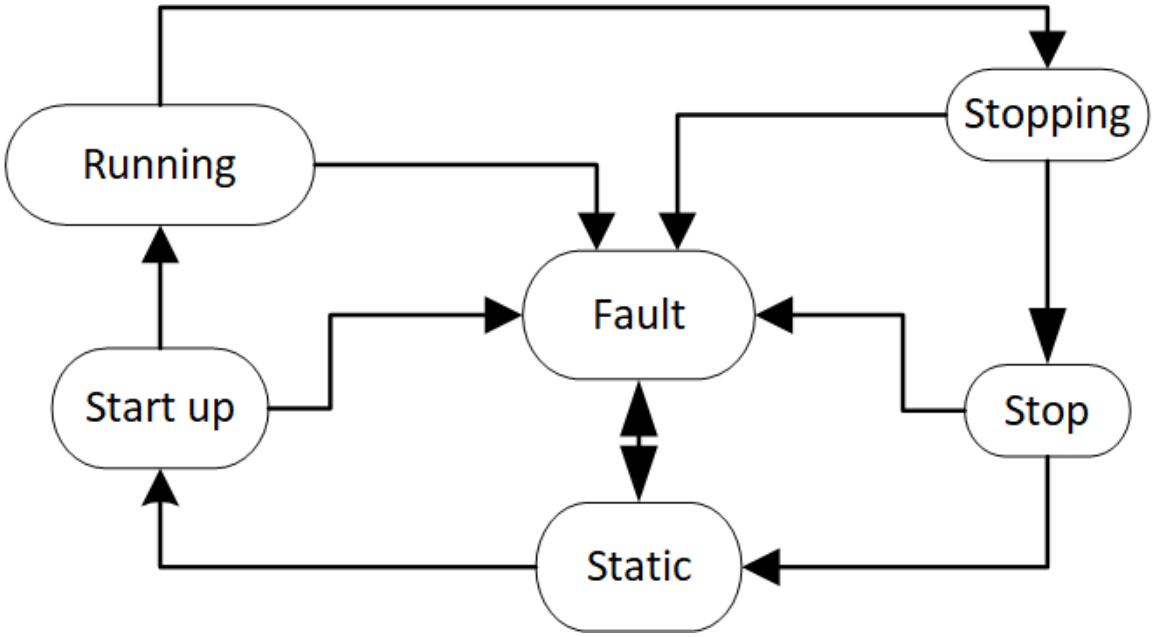

Figure 4.1. The state machine of control system

communicate with one CAN (Controller Area Network) bus peripheral qualified well for our communications protocol.

Table 4.1. Parametrics of dsPIC33EP128MC506

Architecture	16-bit
CPU Speed (MIPS/DMIPS)	128
SRAM (KB)	16
Pin Count	64
Analog Peripherals	1-A/D 16*12-bit
Input Capture	4
SPI	2
Timers	5 x 16-bit 2 x 32-bit
Motor Control PWM Outputs	6
Number of CAN Modules	1

This firmware architecture includes several key routines:

1. Main routine.
2. Timer based task routines.
3. General task routines.
4. Interrupt routines.

4.1.1 Main Routine

Once the control system is powered on, the microcontroller will execute the commands, which have been uploaded in the FLASH. The main routine includes resetting the system and setting up all initial routines. A flow chart of the main routine is shown in Figure 4.2.

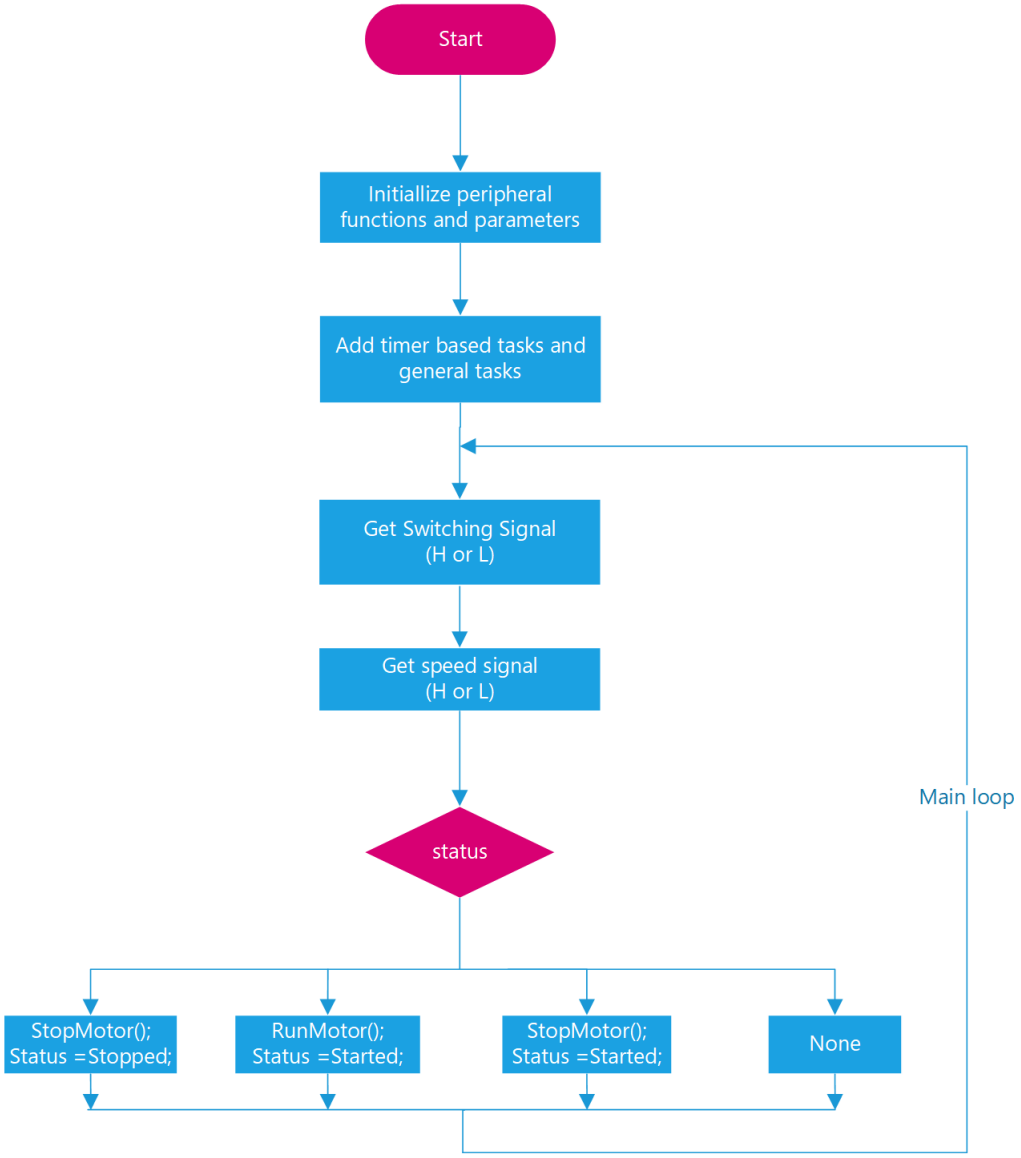

Figure 4.2. Flow chart of main routine

The flow chart indicates that the first thing the controller needs to do is to initialize all peripheral functions and parameters and interrupt settings used in the algorithm. Initialized functions include:

- InitOsc(); - Oscillator and PLL setting
- IOMap();-Mapping the Peripheral pin Selection
- InitADC();-ADC sampling

- InitIC();- Hall sensor inputs interrupt
- InitTMR1(); - TIMR1 for 1K hz interrupt
- InitTMR3(); - Initialize TIMR3 for hall effect capture
- InitPCPWM(); - Set PWM frequency, center aligned mode and dead time
- InitSPI(); - DRV8303 configuration
- InitUART(); - Initialize communication method and speed

Once initialization is ready, the system is waiting for turning on/off and speed high/low depending on the current state.

4.1.2 Interrupt Service Routines

Some events and tasks needs to be executed in interrupt routines due to priority and time restriction. Interrupt task levels need to be arranged based on the priority of the different tasks in case there are interrupt conflicts. The interrupt service routines are listed in Table 4.2. In this program, capture interrupt (IC1) is the highest priority task. Once the Hall effect signal is toggled, system is interrupted and processes this task first in order to get the accurate speed and real time commutation. The microprocessor has a default interrupt priority order, but it can be changed by setting the corresponding register.

Table 4.2. Interrupt Service Routines

Interrupt	When triggered	Task
T1	1 ms	PID control Motor stall protection Timer based task handler
PWM	0.05 ms	Generate PWM frequency
ADC	PWM	current sampling
IC1	HALL A changed	motor commutation rotor speed
IC2	HALL B changed	motor commutation rotor speed
IC3	HALL C changed	motor commutation rotor speed
UART	data received	execute command

4.2 Speed Control Using PID Controller

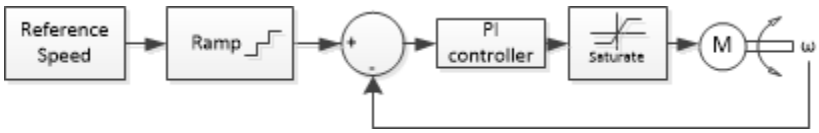

Figure 4.3. Speed feedback control loop

Most regulatory controllers utilize PID closed-loop control. PID controller periodically measures the errors between the reference setpoint value and the measured actual value and applies correction based on the current error (proportional), past cumulative error (integral) and estimate of the future trend (derivative) to achieve tracking of the actual value to the reference setpoint in an efficient manner.

The idea model of the PID controller is presented by this formula:

$$u(t) = K_p e(t) + K_i \int_0^\tau d\tau + K_d \frac{de_t}{dt} \tag{4.1}$$

where,

K_p — is the proportional gain, a tuning parameter,

K_i — is the integral gain, a tuning parameter,

K_d — is the derivative gain, a tuning parameter.

The speed PID control algorithm is implemented in the Timer1 interrupt every 1 millisecond. A person riding the mower may require a certain speed, which is regarded as the reference speed, based on different grass situation. The actual motor speed is measured and obtained in capture interrupt. The difference between the reference and measured speed is the input of PID controller. Figure 4.3 shows how the motor keeps tracking the reference speed. In order to implement in embedded system, the last three errors were saved. It is easier to make equation of the PID controller by changing kp, ki and kd to coefficient values P[0],P[1] and P[2].[29]

$$\begin{aligned} P[0] &= K_p + K_i + K_d \\ P[1] &= -K_p - 2Kd \\ P[2] &= Kd \end{aligned} \tag{4.2}$$

Then PID controller output is:

$$\begin{aligned} Y[n+1] = Y[n] & \\ &+ P[0] \times Error[0] \\ &+ P[1] \times Error[1] \\ &+ P[2] \times Error[2] \end{aligned} \tag{4.3}$$

Kd is the differential parameter. It responds to the rate change of the error signal, but it can produce large output swings, causing an unstable system. It is common

to remove the derivative term from PID control as the Kp and Ki terms are often sufficient to achieve low error and fast response. In such case, the Kd term is set to zero, which is the approach taken for the control system described herein (i.e., PI control rather than PID control)

Figure 2.26 includes the anti windup PI controller, which limits the integral part that causes overshooting. If the PI controller output is saturated (i.e., over the 50V), the integral Ki term is removed to stop the continued addition of the integral in the closed-loop controller. Once the output is the control range, the integral Ki term is added back. Simulation results for PID control with and without anti-windup were compared in the modeling section (Chapter 2).

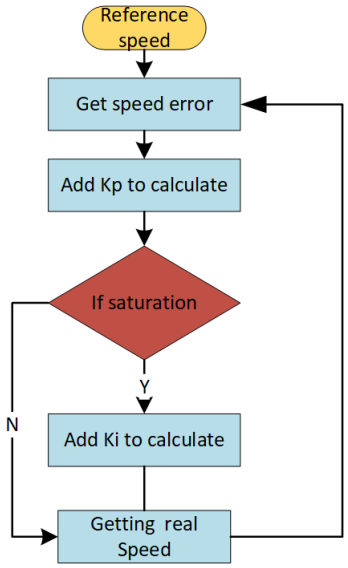

Figure 4.4. PI integral anti windup control

Ramping up the reference speed is also very important. It can prevent generating a very high error to the PID controller. Not ramping the reference speed, especially starting from zero speed, will generate an instantaneous large PWM duty ratio. To address this, a step value is set (shown in Figure 4.5). This step value is added or subtracted to each cycle until the target reference setting is reached. The step accumulation time is set using the timer in microprocessor. Figure 4.6 illustrated

how to implement the speed ramping algorithm. As shown in Figure 4.5, when the system changes speed from 1200 rpm to 3500 rpm, the amount of change per time unit is set as 0.28 rpm every 0.1 millisecond. The change over a 0.13 second time frame is showed in Figure 4.5.

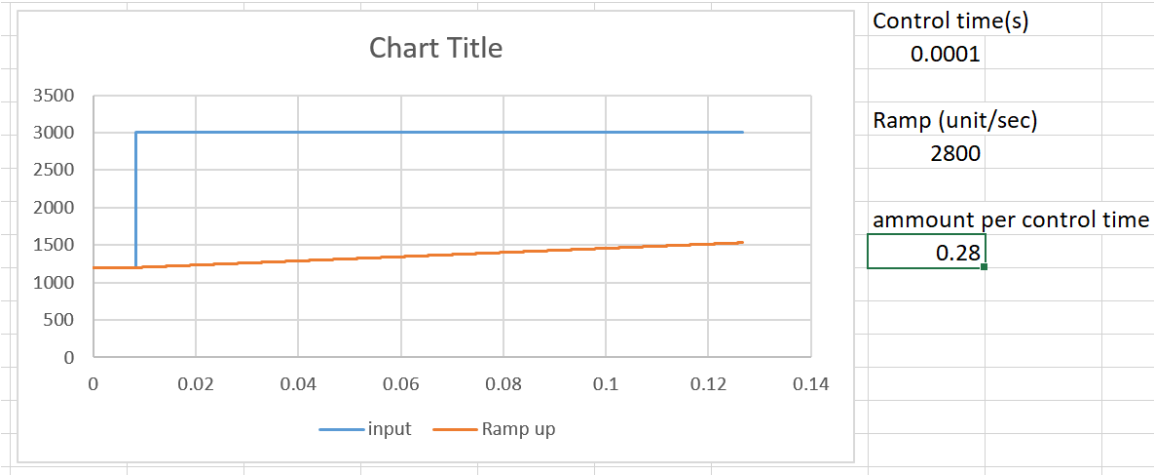

Figure 4.5. Speed ramping up in closed-loop control

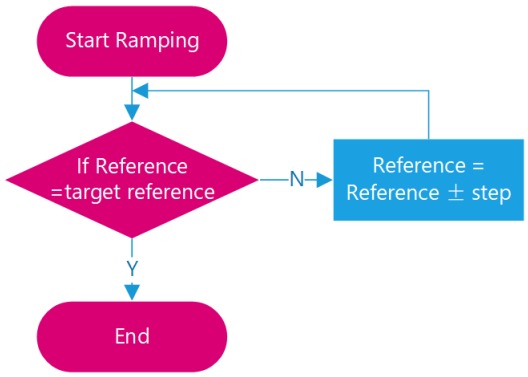

Figure 4.6. Flow chart of speed ramping up

4.3 Low Pass Filter Design

The sampled signal often has noise or disturbance superimposed on the effective signal. This can be addressed not only by adding a hardware low-pass filter, such as an RC filter, but the software can also implement filtering to suppress noise. Filtering

needs to be considered for current and speed sensing to prevent signal distortion. Meanwhile, filtering will cause signal delay. In S domain, the first order low-pass filter transfer function is:

$$H_{(s)} = G\frac{\omega_c}{s+\omega_c} \tag{4.4}$$

In here, Gain G is 1, $\omega_c = 2\pi f$ where f represents the cutoff frequency, which depends on the system noise reduction requirement. 4.4 is the equation for the micro-controller digital filter, which is a first-order digital low-pass filter.

$$y[i] = (1-\alpha)y[i-1] + \alpha x[i] \tag{4.5}$$

Based on cutoff frequency, the corresponding α to implement filtering can be calculated.

$$f_c = \frac{\alpha}{(1-\alpha)2\pi\delta_T} \tag{4.6}$$

Changing Equation 4.5 to Equation 4.7 to avoid floating point calculation is reasonable. In this program, system efficiency is improved by using integer point calculation instead of float calculation.

$$y[i] = y[i-1] - \frac{1}{K}y[i-1] + x[i] \tag{4.7}$$

Where K is an integral value that depends on the cutoff frequency. Figure 4.7 shows the unfiltered signal, as well as signals filtered using Equation 4.5 (with a = 0.95 and 0.98) and Equation 4.7(with K = 20 and 50, respectively). As seen in the figure, when K is equal to 50, the filtered data curves overlap.

Finite Impulse Response (FIR) has some advantages compare to infinite impulse response (IIR), such as requiring no feedback, better stability and ease of designing

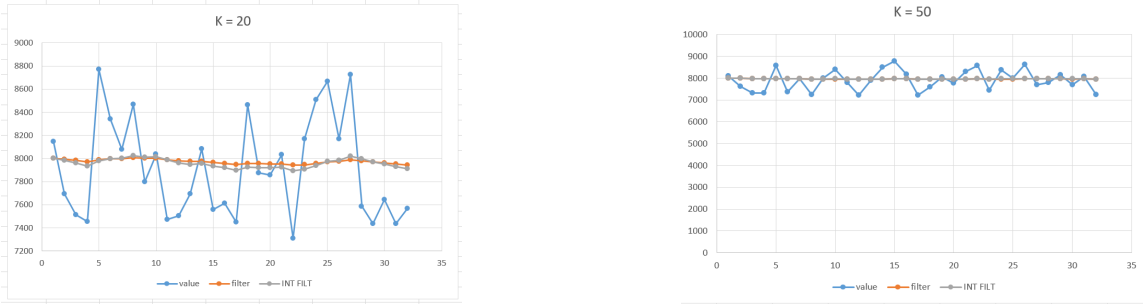

Figure 4.7. Low pass filter by different K

linear phase. For FIR of order N, each value of the output sequence is a weighted sum of the most recent input values:

$$\begin{aligned} y[n] &= a_0 x[n] + a_1 x[n-1] + \cdots + a_N x[n-N] \\ &= \sum_{i=0}^{N} a_i \cdot x[n-i] \end{aligned} \tag{4.8}$$

where:

x[n] is the input signal,

y[n] is the output signal,

N is the filter order;

a_i is a coefficient of the filter.

A moving average filter can be regarded as a simple FIR filter [30]. If a_i in Equation 4.8 are equally divided by N, FIR becomes a moving average filter, such as Equation 4.9:

$$y[i] = \frac{x[n] + x[n-1] + \cdots + x[n-N]}{N} \tag{4.9}$$

In IIR filtering, three variables are used in Equation 4.7. The main disadvantage of FIR filters is that considerably more computation power in a general purpose processor is required compared to that for an IIR filter with similar sharpness or selectivity, especially when low frequency (relative to the sample rate) cutoffs are

needed. In this project, IIR filtering was chosen and the cutoff frequency is set to suppress PWM frequency and other noise.

4.3.1 Hall Position Capture Filter

Three Hall effect sensors always generate six valid position signals. Meanwhile, they also generate the corresponding status based on the last status. Hence, every time the system gets interrupt from IC1, the currently correct signal is measured. 000 and 111 are two invalid statuses. If the last status is 011, the next status should be 010 or 001 based on the running direction. Motor speed can be obtained by calculating the period between two Hall effect signal captures.

4.4 Pulse Width Modulation

DsPIC33 has a certain register related to PWM set up. Typically we set the PWM frequency at 20 kHz to avoid hearing switching noise. Once the frequency is fixed, the phase voltage can be varied by changing the PWM duty cycle. In this six-step control, each time only two MOSFETs turn on, one high side and another low side of different phase. We can use complimentary mode and set up dead time. To reduce switching loss, keep low side always on instead switching and just PWM high side. At this point, we can set low side as normal digital output. Even though complimentary mode is not used, care should be taken to set up set up the dead time register (ALTDTR), which has to be set to a 16 bit positive non-zero value. Otherwise, the PMW duty cycle will become 100% when the program starts, which causes an unexpectedly high current. It is very easy to blow out the MOSFETs in this situation.

4.5 Communication

To communicate with the computer or (human machine interface) HMI, UART (Universal Asynchronous Receiver/Transmitter) communication has been used in this project since UART is the most popular communication tool between system and computer. In microprocessor, Initialize UART (InitUART()) is executed once the micro controller starts. An UART receiving interrupt routine was used in order to receive commands in real time such as start, stop and changing speed.

4.5.1 Graphic User Interface Design

A graphical user interface was designed for feature display and parameter setting, such as duty cycle, speed value, and PI tuning parameters KP and KI.

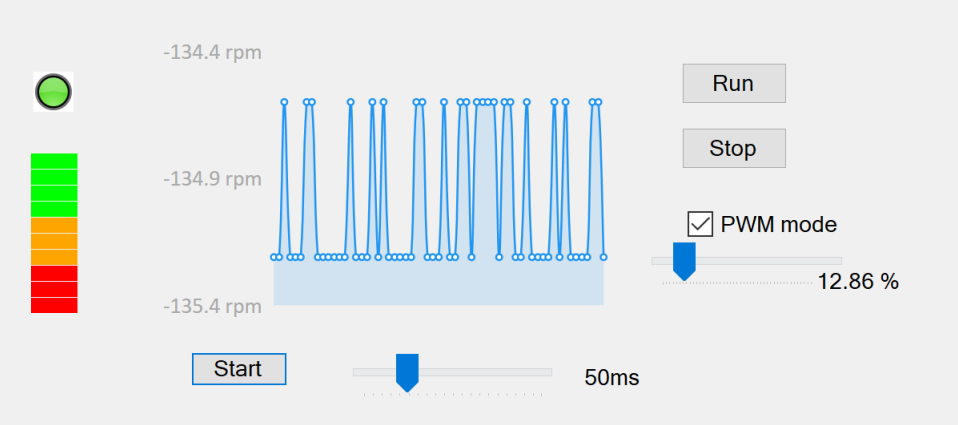

Figure 4.8. Graphic User Interface(GUI) design

There are several features shown in Figure 4.8. The green light blinks every one second (representing heartbeat), which tells the operator whether the system is live. The square bar shows the battery status. Green means full charge and red means low power. When PWM mode is checked, the system operates in open loop mode. The PWM duty cycle can be changed from zero to 100 percent. When PWM mode is unchecked, the system operates in speed closed-loop control. The speed setting can be operated from 0 to 3500 rpm.

5. EXPERIMENTS

5.1 Test Platform and Setting

As described in Chapter 2, the control system was designed for the residential riding mowers. The rated power for the system is 1.5 kW. The rated speed is designed as 2800 rpm. The function and performance of the deck control system was verified through the motor test bench. A hysteresis dynamometer (Magtrol, Buffalo, NY) was used to test the control system according to the manufacturer's instructions [31].

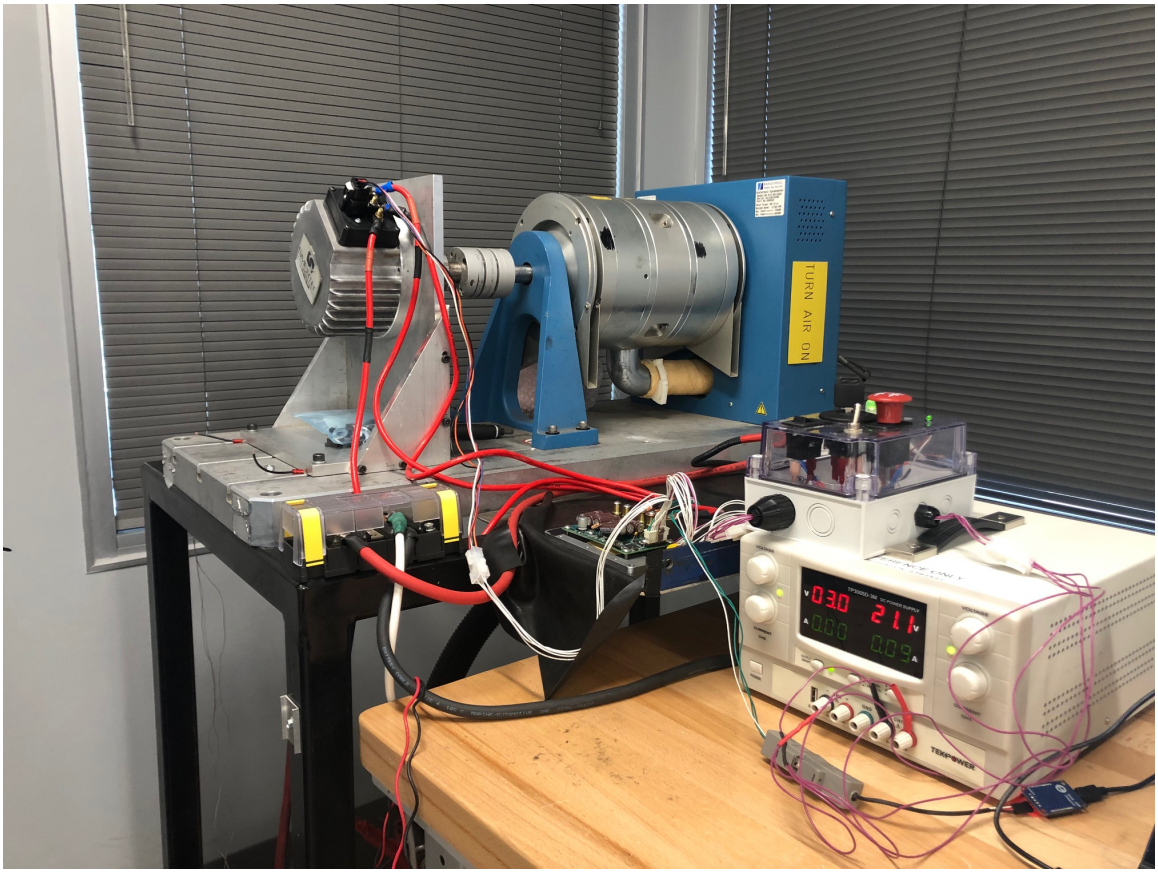

Figure 5.1. Developing test platform

Using a Magtrol motor test bench and Magtrol M-TEST 5.0 (rev. 7.5.2) software (both from Magtrol, Buffalo, NY), different parameters were set up, such as voltage, current, speed and power, etc. As shown in Figure 5.2, the DC voltage power resource was set to 48 V to simulate battery power. The maximum current was set to 50 A. Should overcurrent happen, the test bench will provide overcurrent protection.

Figure 5.2. Test application settings

5.2 Test Result and Test Analysis

The graphical user interface, introduced in Chapter 4.5.1, was used to vary the PWM duty cycle to verify that the program produced the correct output. The PWM duty cycle range can be zero to 100 percent, which is generated by the microprocessor. Figure 5.3 represents 10% and 90% PWM duty cycle outputs.

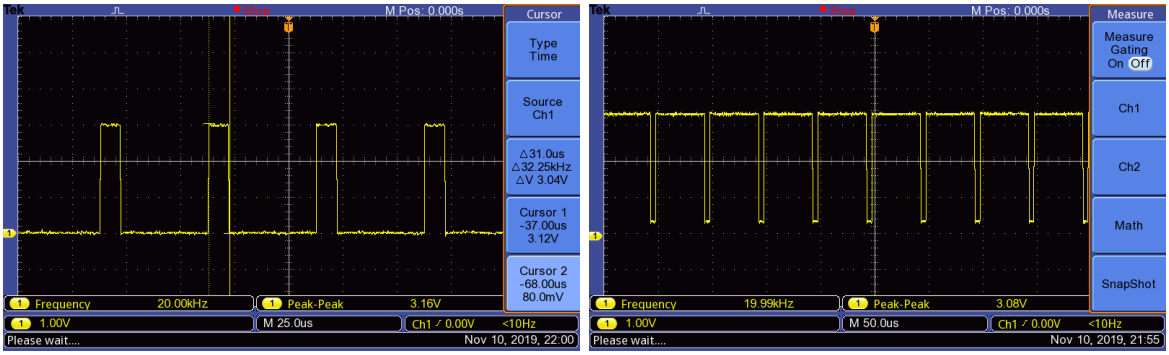

Figure 5.3. PWM output generated from microcontroller

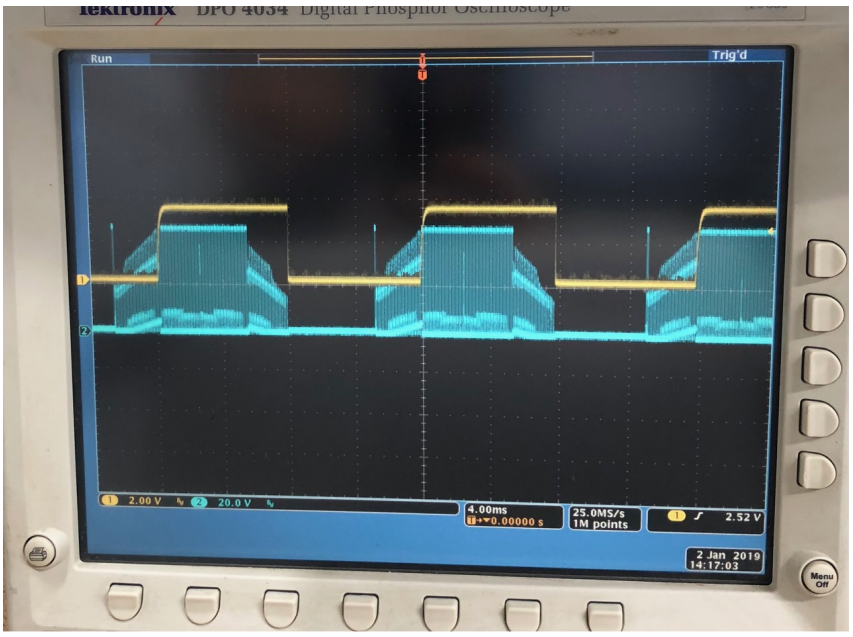

Figure 5.4. Hall effect signal and phase voltage

The Hall effect position signal synchronized with phase commutation. Figure 5.5 displays how these two signals matched. The yellow signal is Hall effect signal A and toggles between 0 and 3.3 V depending on rotor position. The blue signal is the phase A voltage, for which a clear square PWM wave was generated by using

the six-step control algorithm. Because the back electromotive force (BEMF) was influenced by the PWM, a trapezoidal wave was seen instead of a perfect square wave. Additionally, a high voltage peak appeared when the commutation happened. This will be discussed in a later section.

Figure 5.5 shows one of the test results. This test resulted in a motor speed of 3168 rpm, a current of 16.8 A and a torque of 2.14 Nm. This test result matches the six-step control model (discussed in Chapter 2).

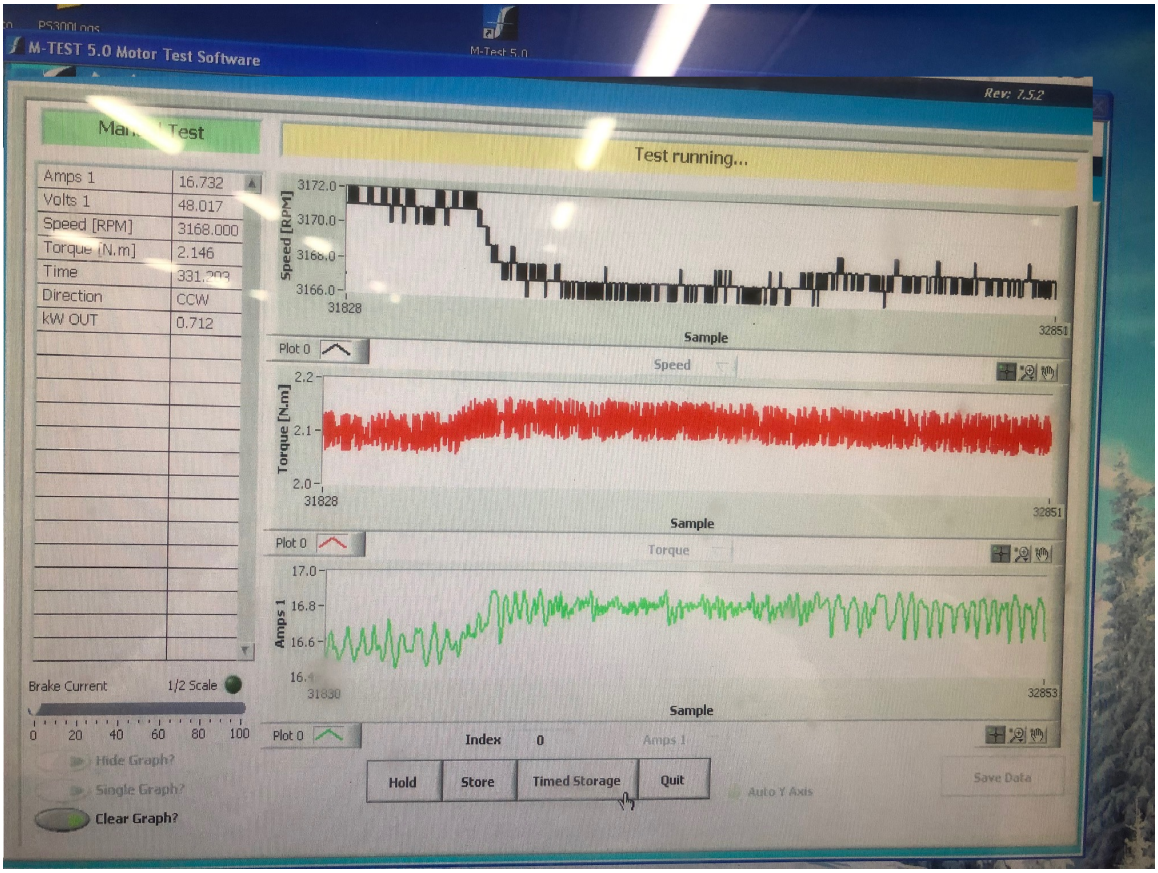

Figure 5.5. Test curve display in MAGTROL

As seen in Figure 5.6, the peak voltage increased when the decreasing the value of R2 and five other same-position resistors (in front of the MOSFETs) (Figure 3.6). R is equal to 33 ohm on the left side, and 50 ohm on the right side. The voltage noise can be mitigated by increasing the resistance value, but this also impacts the PWM

duty cycle. If the value is too large, a 100% duty cycle will not be reached, which reduces the efficiency of the whole system.

Freewheeling time (also called blanking time) will cause a high voltage peak in six-step control. This is shown in Figure 5.7. When commutation happens, which means that the current gets interrupted, the inductive load generates high voltages. In order to get accurate current sampling data, data should be sampled either at PWM on time or at PWM off time. Meanwhile, freewheeling time needs to be avoided. Otherwise, the current samplings will be incorrect. Figure 5.8 shows the blanking time of the falling edge is equal to 64 us when DC link current goes up to 50A in one of the load tests.

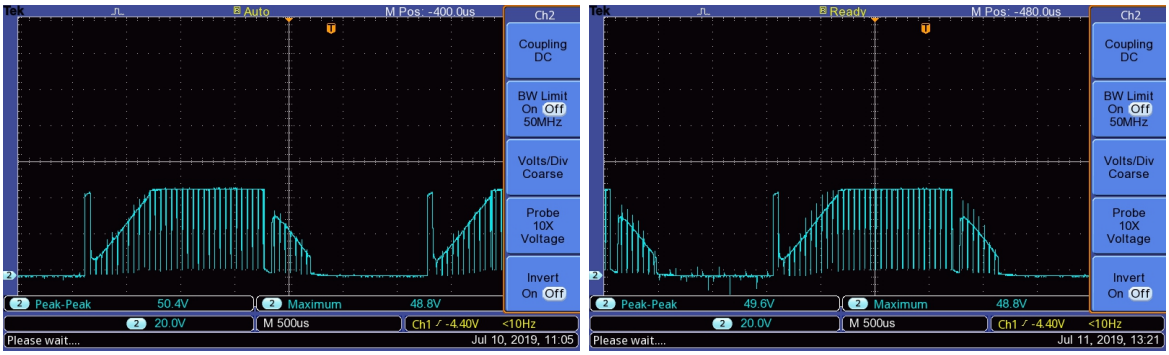

Figure 5.6. Resistance impact the Vdc peak noise

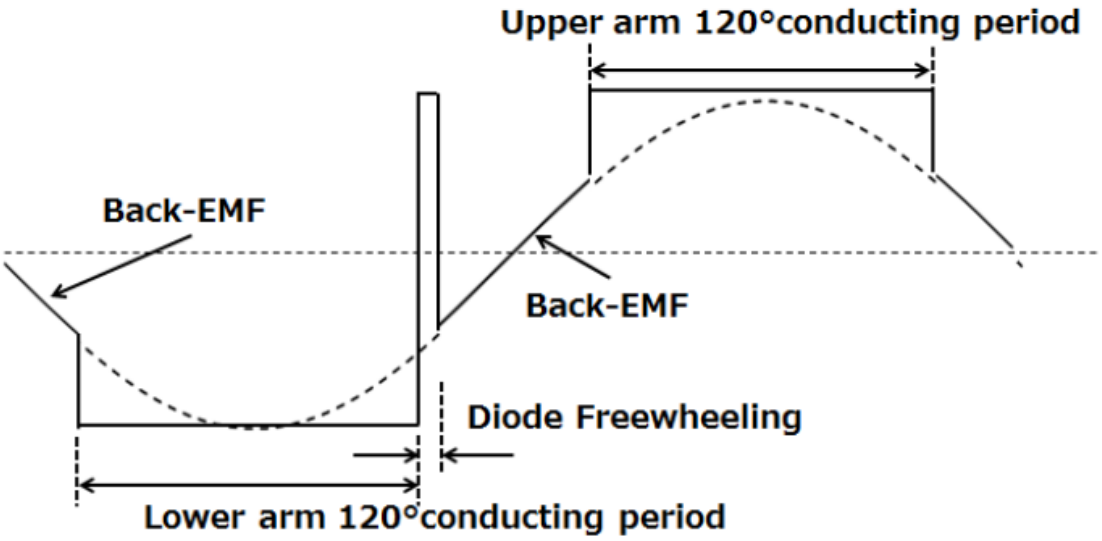

Figure 5.7. Freewheeling display [17]

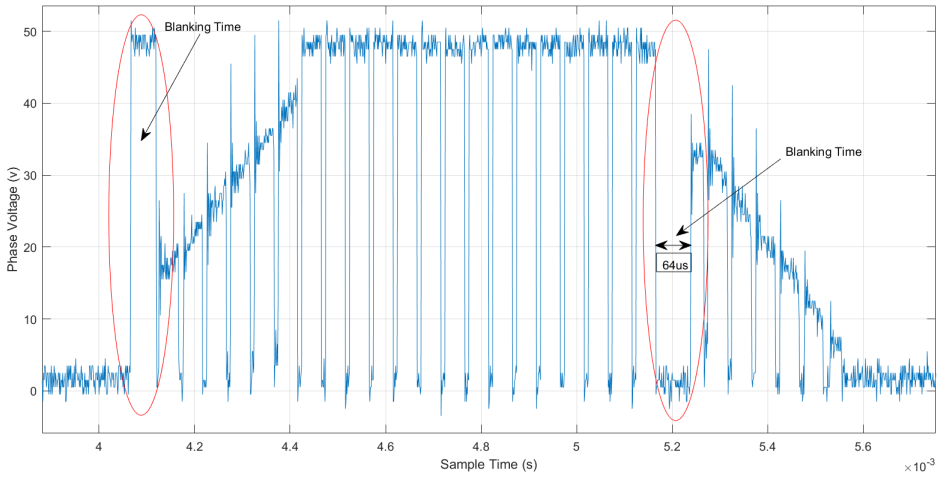

Figure 5.8. Freewheeling display when current goes up to 50A

Heat dissipation is an important factor when designing the controller. A temperature test was performed 5.1 and the test results are shown in Figure 5.9. Three different parts were tested. These were the MOSFETs tab, the heat sink on the other side of the MOSFET, and the edge of the heat sink. Based on a natural logarithmic

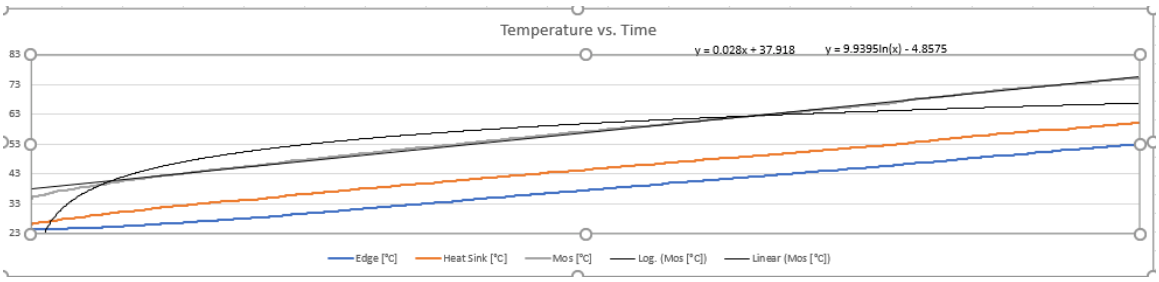

Figure 5.9. Temperature testing chart

trend line function extrapolation, the MOSFET temperature is projected to reach up to 100°C in 180 minutes. Considering the operation temperature of MOSFETs [27], MOSFETs will be broken when temperature is over 150°C.

Table 5.1. MOSFET Temperature Test Result

Current	31 A
Torque	5 Nm
Temp	40 °C
Time Elapsed	235 s
Time to 100°C	6625 s

6. CONCLUSIONS

Modeling, designing and testing of an electric mower deck control system was presented in this thesis. A PMSM-based six-step close loop model built in MATLAB/Simulink provided good guidance for the following physical design. It was necessary to use PWM for phase voltage control to implement speed control. In order to control PMSM flexibly, a microcontroller was used to generate wide-range PWM duty cycle. Digital PID control was implemented in the microcontroller, which made it convenient to tune PID parameters. The main disadvantage of the six-step control is that it generates torque ripple, which is not allowable in some application fields. SPWM and SVPWM models were discussed in the modeling design chapter. The next step is implementation of a closed-loop control system to verify the advantages compared to six-step control. Although six-step control is suitable for the deck control system, it is inevitable that SVM will be used in future work.

REFERENCE

[1] Wikipedia. (2019). Lawn mower, [Online]. Available: https://en.wikipedia.org/wiki/Lawn_mower (Last Date Accessed: 10/18/2019).

[2] B. Okafor, "Simple design of self-powered lawn mower", *International Journal of Engineering and Technology*, vol. 3, no. 10, pp. 933–938, 2013.

[3] (2019). United states electric lawn mower market study 2019: Strategic analysis forecasts 2018-2024 - growing marketing efforts and promotional activities by vendors, [Online]. Available: https://www.globenewswire.com/news-release/2019/03/25/1760048/0/en/United-States-Electric-Lawn-Mower-Market-Study-2019-Strategic-Analysis-Forecasts-2018-2024-Growing-Marketing-Efforts-and-Promotional-Activities-by-Vendors.html (Last Date Accessed: 09/25/2019).

[4] (2019). United states lawn mower market analysis & forecasts 2019-2024: Shifting consumer focus toward smart technology and emergence of robotic lawn mowers, [Online]. Available: https://www.prnewswire.com/news-releases/united-states-lawn-mower-market-analysis-forecasts-2019-2024-shifting-consumer-focus-toward-smart-technology--emergence-of-robotic-lawn-mowers-300819523.html (Last Date Accessed: 09/20/2019).

[5] A. Christensen, R. Westerholm, and J. Almén, "Measurement of regulated and unregulated exhaust emissions from a lawn mower with and without an oxidizing catalyst: A comparison of two different fuels", *Environmental science & technology*, vol. 35, no. 11, pp. 2166–2170, 2001.

[6] N. Singh and S. C. Davar, "Noise pollution-sources, effects and control", *Journal of Human Ecology*, vol. 16, no. 3, pp. 181–187, 2004.

[7] J. P. Chambers, "Noise pollution", in *Advanced air and noise pollution control*, Springer, 2005, pp. 441–452.

[8] J. A. G. Balanay, G. D. Kearney, and A. J. Mannarino, "Assessment of occupational noise exposure among groundskeepers in north carolina public universities", *Environmental health insights*, vol. 10, EHI–S39682, 2016.

[9] S. Derammelaere, M. Haemers, J. De Viaene, F. Verbelen, and K. Stockman, "A quantitative comparison between bldc, pmsm, brushed dc and stepping motor technologies", in *2016 19th International Conference on Electrical Machines and Systems (ICEMS)*, Ieee, 2016, pp. 1–5.

[10] R. Krishnan, *Permanent magnet synchronous and brushless DC motor drives*. CRC press, 2017.

[11] T. M. Jahns, "Flux-weakening regime operation of an interior permanent-magnet synchronous motor drive", *IEEE Transactions on Industry Applications*, no. 4, pp. 681–689, 1987.

[12] Q. Yi, D. Shen, J. Lin, S. Chien, L. Li, Y. Chen, and R. Sherony, "Color and height characteristics of surrogate grass for the evaluation of vehicle road departure mitigation systems", SAE Technical Paper, Tech. Rep., 2019.

[13] E. L. C. Arroyo, "Modeling and simulation of permanent magnet synchronous motor drive system", *University of puerto rico, Mayagüez Campus*, 2006.

[14] T. Husain, I. Hasan, Y. Sozer, I. Husain, and E. Muljadi, "Design of a modular e-core flux concentrating transverse flux machine", *IEEE Transactions on Industry Applications*, vol. 54, no. 3, pp. 2115–2128, 2018.

[15] J. R. Hendershot and T. J. E. Miller, *Design of brushless permanent-magnet machines*. Motor Design Books, 2010.

[16] Wikipedia. (2019). Dc injection braking, [Online]. Available: https://en.wikipedia.org/wiki/DC_injection_braking (Last Date Accessed: 11/18/2019).

[17] Toshiba. (2018). 120° square-wave commutation for brushless dc motors, [Online]. Available: https://toshiba.semicon-storage.com/info/docget.jsp?did=61176 (Last Date Accessed: 11/03/2019).

[18] A. Nahar. (2013). Bldc motor drive system, [Online]. Available: https://www.slideshare.net/anahar/bldc-motor-drive-system (Last Date Accessed: 08/05/2019).

[19] D. Yuan, *Permanent Magnet Synchronous VF system and control*. China Machine Press, 2015.

[20] S. Allirani and V. T. Raaj, "Development of space vector pulse width modulation algorithm for voltage source inverter using dspic controller 30f4011", *International Journal of Pure and Applied Mathematics*, vol. 114, no. 9, pp. 257–269, 2017.

[21] Microchip. (2005). Vf control of 3-phase induction motor using space vector modulation, [Online]. Available: http://ww1.microchip.com/downloads/en/Appnotes/00955a.pdf (Last Date Accessed: 11/01/2019).

[22] T. Trip. (2019). Space vector pulse width modulation(svpwm), simulation in simulink 2015, [Online]. Available: https://www.youtube.com/watch?v=qysCTtKNShw (Last Date Accessed: 08/05/2019).

[23] A. MANSURI. (2013). Space vector modulation, [Online]. Available: https://www.mathworks.com/matlabcentral/fileexchange/70455%20space%20vector%20modulation (Last Date Accessed: 06/02/2019).

[24] Microchip. (2010). Sensorless field oriented control of a pmsm, [Online]. Available: https://www.microchip.com/wwwAppNotes/AppNotes.aspx?appnote=en530042 (Last Date Accessed: 10/04/2019).

[25] W. Deng and S. Zuo, "Comparative study of sideband electromagnetic force in internal and external rotor pmsms with svpwm technique", *IEEE Transactions on Industrial Electronics*, vol. 66, no. 2, pp. 956–966, 2018.

[26] S. Lin, T. Wu, L. Zhou, F. Moslehy, J. Kapat, and L. Chow, "Modeling and design of super high speed permanent magnet synchronous motor (pmsm)", in *2008 IEEE National Aerospace and Electronics Conference*, IEEE, 2008, pp. 41–44.

[27] IXYS. (2017). Three phase full bridge - ixys power, [Online]. Available: http://ixapps.ixys.com/Datasheet/MTI85W100GC.pdf (Last Date Accessed: 06/14/2019).

[28] T. INSTRUMENTS. (2016). Ina240 high- and low-side, bidirectional, zero-drift, current-sense amplifier with enhanced pwm rejection, [Online]. Available: http://www.ti.com/lit/ds/symlink/ina240.pdf (Last Date Accessed: 11/01/2019).

[29] J. Zambada, "Sinusoidal control of pmsm motors with dspic30f dsc", *Microchip Technology Inc*, 2005.

[30] Mathuranathan. (2010). Moving average filter (ma filter), [Online]. Available: https://www.gaussianwaves.com/2010/11/moving-average-filter-ma-filter-2/ (Last Date Accessed: 10/23/2019).

[31] Magtrol. (2018). Hd and ed series hysteresis dynamometers, [Online]. Available: https://www.magtrol.com/wp-content/uploads/hdmanual.pdf (Last Date Accessed: 10/01/2019).